

UNIVERSIDAD POLITÉCNICA DE MADRID  
Escuela Técnica Superior de Ingenieros de Caminos, Canales y  
Puertos



**Mechanical Behaviour and Numerical  
Modelling of Uncured Prepreg Composites for  
Thermoforming Processes**

**DOCTORAL THESIS**

Submitted for the degree of Doctor by:

**Jorge David Aveiga García**  
M.Sc. in Aeronautical Engineering

Madrid, 2023



UNIVERSIDAD POLITÉCNICA DE MADRID  
Escuela Técnica Superior de Ingenieros de Caminos, Canales  
y Puertos

**Doctoral Degree in Engineering of Structures, Foundations and  
Materials**

**Mechanical Behaviour and Numerical  
Modelling of Uncured Prepreg Composites for  
Thermoforming Processes**

**DOCTORAL THESIS**

Submitted for the degree of Doctor by:

**Jorge David Aveiga García**  
M.Sc. in Aeronautical Engineering

Under the supervision of:  
Dr. Carlos Daniel Gonzalez Martinez

Madrid, 2023

Title: Mechanical Behaviour and Numerical Modelling of Uncured Prepreg Composites for Thermoforming Processes

Author: Jorge David Aveiga García

Doctoral Programme: Engineering of Structures, Foundations and Materials

Thesis Supervision:

Dr. Carlos Daniel González Martínez, Catedrático de Universidad, ETS de Ingenieros de Caminos, Canales y Puertos, Universidad Politécnica de Madrid.(Supervisor)

External Reviewers:

Thesis Defense Committee:

Thesis Defense Date:



## Acknowledgement

The four years a student spends pursuing the desired doctoral degree are filled with innumerable highs and lows, and throughout those times, there are people who come into our lives and lend a helping hand in both professional and emotional ways. I'd like to start by thanking my loved ones who have been by my side unconditionally despite the thousands of kilometres that separate us: my parents Luis and Janeth, my siblings Elaine, Daniela, and Israel, my grandmother Delia, my brother-in-law Eduardo, my niece, and all my nephews who make up my close family circle, whose voices and hugs have been present throughout this long process.

My project supervisor and thesis tutor, Professor Carlos González, deserves a large share of my gratitude for his consistent mentoring throughout this process and for helping to mould my future professional and academic career. At this point, I would like to remember Professor Cláudio Lopes, whose image and guidance have been present in the development of this work, as he was the first to repose his trust in me during the doctorate. My gratitude also extends to the post-doctorates Angel León, David Garoz, Mario Rueda, and Davide Mocerino, as well as the laboratory technicians Vanesa Martínez, José Luis Jimenez, José Sánchez, Miguel de la Cruz, and Javier García, who worked side by side with me and actively contributed to the development of this thesis. Without a doubt, I would like to express my gratitude to all of the coworkers and friends who collaborated with me in the Structural Composites group between 2019 and 2023, as well as to the coworkers from other IMDEA groups who I had the pleasure of sharing the stage with at the institute and on our meetings, bars, and trips we took together. Lastly, I would like to express my sincere gratitude to the Instituto Madrileño de Estudios Avanzados, IMDEA Materials, for providing me with the opportunity to complete my doctorate research there. The realisation of this research would not have been feasible without the financial support and collaboration from FIDAMC through the TEMACOM project, to whom I am very grateful.

# Abstract

The progress in aircraft structures is influenced not only by the search for novel materials but also by the development and improvement of manufacturing techniques. Considerable focus has been placed on the revolutionary advantages of composite materials in improving the effectiveness and weight-bearing capabilities of aerospace structures. However, it is crucial to emphasise the changes in production techniques that accompany these innovative materials. These changes have also triggered a revolution in aerospace workshops. A valuable use of these composite materials is in the form of pre-impregnated sheets, which consist of fibres embedded in resin, each possessing distinctive compositions. This material, also referred to as "prepreg", optimises the fibre/matrix ratio while speeding the layering procedure for laminates. This improvement results in greater mechanical performance and less waste compared to alternative solutions.

The process of manufacturing an aircraft component from prepreg entails several sequential steps: layering, heating, moulding, consolidation, curing, and demoulding. Every stage possesses its own distinct array of technologies. This thesis explores the thermoforming manufacturing method, which is widely adopted in the modern aerospace industry. Thermoforming is a process that entails using heat to shape a pre-laminated, uncured prepreg onto a mould and then using pressure to consolidate it. This approach effectively covers the heating, moulding, and consolidation stages, resulting in structurally complex single components, minimising the requirement for mechanical joints. Yet, for all its adaptability, thermoforming with uncured prepregs has certain constraints. Imperfections such as wrinkles, folds, and uneven thickness might degrade the effectiveness of the component, presenting a difficulty in guaranteeing constant quality.

In this research, we provide a comprehensive mechanical analysis of the uncured AS4/8552 prepreg, an area not extensively documented in the scientific literature. Addressing the challenges encountered during mechanical testing of these laminates, we introduce novel modifications to standard experimental methods. These modifications involve incorporating new processing phases into the manufacture of test samples. The findings are substantial and provide a basis for an initial attempt to create a mathematical material model that can be used for computational simulations. A novel viscoelastic material model is introduced, implementing the equations that describe a generalised Maxwell element. The study concludes that the interaction between the laminate layers and the degree of movement freedom they possess while not cured is responsible for a sizable fraction of the imperfections in the laminate.

# Resumen

El progreso en las estructuras aeronáuticas no solo es influenciado por la búsqueda de nuevos materiales, sino también por el desarrollo y mejora de técnicas de fabricación. Se ha puesto considerable énfasis en las ventajas revolucionarias de los materiales compuestos para mejorar la eficacia y la capacidad de carga de las estructuras aeroespaciales. Sin embargo, es esencial resaltar los cambios en las técnicas de producción que acompañan a estos materiales innovadores. Estos cambios también han desencadenado una revolución en los talleres aeroespaciales. Un valioso uso de estos materiales compuestos se encuentra en la forma de láminas pre-impregnadas, que consisten en fibras embebidas en resina, ambos con composiciones distintas. Este material, también referido como "prepreg", optimiza la relación fibra/matriz y acelera el procedimiento de apilamiento de láminas. Esta mejora resulta en un elevado rendimiento mecánico y menos residuos en comparación con otras técnicas de fabricación.

El proceso de fabricación de un componente aeronáutico a partir de prepreg implica varios pasos secuenciales: apilamiento, calentamiento, moldeo, consolidación, curado y desmoldeo. Cada etapa posee su propio conjunto distinto de tecnologías. Esta tesis explora el método de fabricación de termoformado, que es ampliamente adoptado en la industria aeroespacial moderna. El termoformado es un proceso que implica usar calor para dar forma a un prepreg pre-laminado y no curado sobre un molde, y luego usar presión para consolidarlo. Este enfoque cubre eficazmente las etapas de calentamiento, moldeo y consolidación, resultando en componentes estructuralmente complejos, minimizando la necesidad de juntas mecánicas. Sin embargo, a pesar de toda su adaptabilidad, el termoformado con prepregs no curados tiene ciertas limitaciones. Imperfecciones como arrugas, pliegues y espesores desiguales pueden degradar la eficacia del componente, presentando un desafío para garantizar una calidad constante.

En esta investigación, proporcionamos un análisis mecánico exhaustivo del prepreg no curado AS4/8552, un área no ampliamente documentada en la literatura científica. Abordando los desafíos encontrados durante las pruebas mecánicas de estos laminados, introducimos modificaciones novedosas a los métodos experimentales estándar. Estas modificaciones involucran la incorporación de nuevas fases de procesamiento en la fabricación de muestras de prueba. Los hallazgos son sustanciales y proporcionan una base para un primer intento de crear un modelo matemático de material que pueda usarse para simulaciones computacionales. Se introduce un nuevo modelo material viscoelástico, implementando las ecuaciones que describen un elemento Maxwell generalizado. El estudio concluye que la interacción entre las capas del laminado y el grado de libertad de movimiento que poseen cuando no están curados es responsable de una fracción significativa de las imperfecciones en el laminado.



# Table of Contents

Acknowledgement . . . . .	iii
Abstract . . . . .	iv
Resumen . . . . .	v
List of Figures . . . . .	viii
List of Tables . . . . .	xiii
<b>1 Synopsis of Composite Materials and Manufacturing Methods</b>	<b>1</b>
1.1 The Reinforcement Fibres . . . . .	2
1.2 The Matrices . . . . .	4
1.3 Manufacturing Methods for Polymer Matrix Composites . . . . .	5
1.3.1 Injection Moulding . . . . .	7
1.3.2 Resin Transfer Moulding (RTM) . . . . .	8
1.3.3 Filament Winding (FW) . . . . .	8
1.3.4 Additive Manufacturing . . . . .	9
1.4 Preimpregnated composites and its applications in aerospace engineering. . .	10
1.5 Thermoforming manufacturing to produce thermoset prepreg composites . .	13
1.5.1 Thermoforming process . . . . .	15
1.5.2 Thermoforming: Wrinkles and Defects . . . . .	16
1.6 Aims and scopes . . . . .	18
<b>2 Materials and experimental techniques for the mechanical characterisation of uncured prepreps</b>	<b>19</b>
2.1 Material . . . . .	19
2.2 Mechanical characterisation of cured prepreg laminates . . . . .	20
2.3 Mechanical characterisation of uncured prepreg laminates . . . . .	24
2.3.1 Intraply behaviour of uncured prepreg laminates . . . . .	24
2.3.2 Partial curing device . . . . .	30
2.3.3 A rheometer-based tensile test . . . . .	34
2.4 Mechanical characterisation of interply behaviour of uncured prepreg composites	36
2.4.1 Pull-out test and friction measurements . . . . .	36
2.5 Compaction analysis of uncured prepreg composite laminates . . . . .	40
2.6 2-point flexural test of uncured composite laminates . . . . .	43
2.6.1 Components analysis of the bending device . . . . .	43
2.6.2 Test Execution and Data Processing . . . . .	45

<b>3</b>	<b>Experimental Results</b>	<b>49</b>
3.1	In-plane Mechanical Characterisation . . . . .	49
3.1.1	Longitudinal Stress Test . . . . .	49
3.1.2	Transverse Stress Test . . . . .	50
3.1.3	Shear Stress Test . . . . .	54
3.2	Results of the pull-out test and calculations of the friction coefficients . . . . .	57
3.2.1	Friction Interpretation and Interlayer Measurements . . . . .	62
3.3	Compaction test results . . . . .	65
3.4	2-point bending test analysis . . . . .	70
3.5	$\pm 30^\circ$ and $\pm 60^\circ$ Off-axis Test: Results and Comparison . . . . .	73
<b>4</b>	<b>Modelling the mechanical behaviour of uncured composite materials</b>	<b>77</b>
4.1	Advancements in Mathematical Modeling of Uncured Prepreg Composites . . . . .	77
4.2	Formulation for an anisotropic fibre-reinforced viscoelastic material model . . . . .	80
4.2.1	Validation and implementation of the VUMAT . . . . .	83
4.2.2	Simulation of the $[\pm 45]_{2s}$ experimental case . . . . .	84
4.3	Interply friction modelling: lubrication theory . . . . .	86
4.3.1	Resolution of the Reynolds equation . . . . .	90
4.4	Thermoforming Modeling . . . . .	91
<b>5</b>	<b>Conclusions and Future Work</b>	<b>95</b>
5.1	Conclusions . . . . .	95
5.2	Future research . . . . .	98
	<b>References</b>	<b>101</b>

# List of Figures

1.1	First aeroplanes to use glass fibre composite. Copyright information: . . . . .	2
1.2	The aircrafts in (a) and (b) were the first to incorporate CFRP in their construction, accounting for 13% of the overall weight, whereas (c) and (d) are more recent models with a structural composite content of 55%. <i>Copyright ©: a) Guilherme Irber, b) Charles Cunliffe, c) Mark Van der Vliet and d) Vyacheslav Firsov.</i> . . . . .	3
1.3	An synopsis of all composite manufacturing processes organised by the kind of resin and fibre used (Pantelakis, 2020). . . . .	7
1.4	Illustration of Injection Moulding . . . . .	8
1.5	Simplified RTM system for manufacture of composite components . . . . .	9
1.6	An illustration of the winding of a filament (Mallick, 2007). . . . .	10
1.7	Example of the concurrent use of composites manufacturing and additive manufacturing. <i>Copyright ©Electroimpact.</i> . . . . .	10
1.8	Hot Melt Process for prepreg production. . . . .	12
1.9	Solvent Dip Process for prepreg production. . . . .	13
1.10	Illustration of the hand lay-up procedure (Buragohain, 2017). . . . .	14
1.11	Diagram of a standard dispensing head for Automated Tape Laying (ATL) and Automated Fibre Placement (AFP) machines (Falzon and Pierce, 2020). . . . .	15
1.12	Thermoforming process of prepreg sheets including a thermal diagram (Guzman-Maldonado et al., 2016). . . . .	16
1.13	Regular wrinkles noticed during thermoforming of composite plies. These irregularities lead to undesired displacements, reorientation of the fibres, and warping (Slange, 2019; Wolthuizen et al., 2014). . . . .	17
2.1	Characterisation method . . . . .	20
2.2	Material axis for fiber-reinforced composite ply schematic (Chen et al., 2018). . . . .	21
2.3	Schematic representation of the different testing procedures for the compressive test: a) End Loading, b) Shear Loading, c) Combined Loading. . . . .	23
2.4	Most typical types of bending tests in the literature: a) Three-Point Bending Test and b) Four-Point Bending Test. Both correspond to the standard ASTM D7264, 2015. . . . .	23
2.5	Different Shear Test methods available in the literature: a) $\pm 45^\circ$ off-axis Tensile Shear Test, b) V-Notched Test, c) Rail Shear Test, d) The Iosipescu and e) $10^\circ$ off-axis Tensile Shear Test. . . . .	24

2.6	Typical failures of uncured prepreg coupons: a) Transverse Tensile samples ( $[90^\circ]$ ) fail due to the resin's poor strength resistance, and b) Longitudinal Tensile samples ( $[0^\circ]$ ) consistently fail at the tab zone. . . . .	25
2.7	a) Dynamic Mechanical Analysis of a prepreg sample subjected to periodic cantilever beam deflection and b) Temperature dependence of the 8552 epoxy viscosity. . . . .	26
2.8	Stress-strain response of Normal Tensile test while modifying the thickness of the laminate by using 1, 2, and 4 plies. . . . .	27
2.9	Double Notched Test modification for uncured prepreg composite samples: a) The presence of fibre bridgings in the samples, and b) The torsion effect caused by the fibre bridging. . . . .	28
2.10	$10^\circ$ off-axis Tensile Shear Test of uncured prepreg composite laminates. a) Test sample displaying the $10^\circ$ inclination of the sheared zone after testing. c) Test results at three temperatures (RT, $40^\circ\text{C}$ , and $60^\circ\text{C}$ ) and three displacement rates (0.5, 1, and 2 mm/min). . . . .	29
2.11	Partial curing device to produce multiaxial tensile coupons for mechanical characterisation. . . . .	31
2.12	$[\pm 45^\circ]_{ns}$ tensile tests ( $n = 2, 4, 8$ ): a) specimens with the uncured gripping area, b) specimens with the cured gripping area, c) DIC analysis of samples 16 plies and uncured tabs and, d) DIC analysis of samples 16 plies and cured tabs. . . . .	33
2.13	Tensile test samples after curing the tabs: a) Normal tensile test with stacking sequence of $[0^\circ]_8$ , b) Transverse tensile test with stacking sequence of $[90^\circ]_8$ , and c) $\pm 45^\circ$ stacking - curing shear tensile test with stacking sequence of $[\pm 45^\circ]_{2s}$ . . . . .	34
2.14	Rheometer apparatus for tensile tests: a) Modular Compact Rheometer MCR 702e, b) Temperature sensor positioned directly within the measurement system, and c) High-precision temperature control device with optoelectronic technology. . . . .	35
2.15	Samples used in the rheometer-based tensile test. A sample after testing is shown on top, while two untested samples are seen at the bottom. . . . .	36
2.16	a) Experimental set-up used for measuring friction coefficient, b) Test for prepreg-tool friction measurement, c) Test for prepreg-prepreg friction measurement. . . . .	39
2.17	a) A fixture for the compaction test with two parallel plates mounted on a universal testing machine. b) A typical load vs displacement plot from the compaction test, displaying the fibre bed curve. . . . .	41
2.18	A visual representation of load and displacement curves plotted against time, providing insight into the displacement cycle and the corresponding load readings. . . . .	42
2.19	The two-points bending test (2PBT). a) Room temperature configuration and b) Increased temperature adaptation. . . . .	44
2.20	Real-time reading of bending test in progress. a) Angle variation over time due to weight increases as captured by the sensor. b) Estimation of sample curvature by fitting captured image coordinates at each weight increment. . . . .	46
2.21	a) The presence of observable wrinkles on the surface of the sample, b) a standardised weight of 100g, and c) the positioning of the sample with the edges placed within the notches. . . . .	47

2.22	The camera frame captured during the testing process exhibits the upper portion of the sample, together with a longitudinal side view that shows a set of guiding marks. . . . .	48
3.1	Stress-Strain curve for the normal tensile test at 22°(RT), 40°, and 60°. . . .	50
3.2	Mismeasurement of the transverse tensile test being conducted with the Instron universal testing machine together with a temperature chamber. a) Test conducted at 40°C degrees Celsius, and b) Test conducted at 60°C degrees Celsius. . . . .	51
3.3	Comparative analysis of the stress vs strain response of a sample tested at room temperature with a strain rate of 2 mm/min using Rheometer and Universal testing machine. . . . .	51
3.4	Stress-strain response of the transverse tensile test. a) The experiment was conducted at room temperature employing a universal testing machine to apply three different strain rates. b) The experiment was carried out at a temperature of 40°C using a rheometer to apply three different strain rates. c) The experiment was conducted at 40°C using a rheometer to apply three different strain rates. . . . .	52
3.5	The viscosity's behaviour. a) Shear stress response dependent on shear rate, and b) Newtonian and non-Newtonian viscosity behaviour. . . . .	54
3.6	[±45] <sub>2s</sub> Shear Tensile Test employing a universal testing machine at three different strain rates. a) Test conducted at RT, b) Test conducted at a temperature of 40°C and c) Test conducted at a temperature of 60°C. . . . .	55
3.7	Pull-out load curves $F - U$ for prepreg-prepreg friction ( <b>a-f</b> ) and for prepreg-tool friction ( <b>g-n</b> ) tests carried out at 40 °C and 60 °C with pressure and sliding velocities ranging between 0.5–2 bars and 1–10 mm/min. . . . .	58
3.8	Average friction coefficient and standard deviation at 40 °C and 60 °C for prepreg-prepreg contact in ( <b>a,b</b> ) and prepreg-tool contact in ( <b>c,d</b> ). . . . .	59
3.9	Stribeck curves for the friction coefficient: (a) Prepreg-prepreg contact, (b) Prepreg-tool contact. . . . .	63
3.10	Optical micrographs of the contact surfaces after testing. In ( <b>a,b</b> ) is presented prepreg-prepreg contact surfaces for 40 °C and 60 °C; in ( <b>c,d</b> ) prepreg-tool contact surfaces respectively for 40 °C and 60 °C. Coupons were tested at 1 mm/min sliding speed. . . . .	64
3.11	( <b>a</b> ) XCT reconstruction of [0°] <sub>8</sub> laminates for the interlayer thickness determination, ( <b>b</b> ) SEM image with a detailed view of the space between two adjacent prepreg plies, ( <b>c</b> ) Average resin interlayer thickness as a function of the temperature and applied pressure. . . . .	65
3.12	Comparison of load vs displacement response of AS4/8552 prepreg composite with different stacking sequences, assessed under compaction forces at room temperature A fitted red curve representing the fibre bed effect is shown in the plot. . . . .	66
3.13	Comparison of load vs displacement response of AS4/8552 prepreg composite with different stacking sequences, assessed under compaction forces at 40°C. A fitted red curve representing the fibre bed effect is shown in the plot. . . . .	67

3.14	Comparison of load vs displacement response of AS4/8552 prepreg composite with different stacking sequences, assessed under compaction forces at 60°C. A fitted red curve representing the fibre bed effect is shown in the plot. . . . .	68
3.15	The loading cycle of a 2-points bending test and the reduction of the curvature ratio as the sample is being bent. The test corresponds to an 8-layer uncured prepreg laminate being tested at room temperature." . . . . .	71
3.16	Sequencing the formation of wrinkling in an uncured prepreg laminate under bending loading. Time and loading identification for each occurrence. . . . .	72
3.17	$[\pm 30]_{2s}$ Shear Tensile Test employing a universal testing machine at three different strain rates. a) Test conducted at RT, b) Test conducted at a temperature of 40°C and c) Test conducted at a temperature of 60°C. . . . .	73
3.18	$[\pm 60]_{2s}$ Shear Tensile Test employing a universal testing machine at three different strain rates. a) Test conducted at RT, b) Test conducted at a temperature of 40°C and c) Test conducted at a temperature of 60°C. . . . .	74
3.19	A comparison of stress levels and viscoelastic response was conducted on samples with four different fibre directions at room temperature. . . . .	75
4.1	A fibre bundle displaying slight waviness . . . . .	79
4.2	Recognition of the mechanics of resin flow during the forming process . . . . .	79
4.3	Abaqus model with a single element for validating the user subroutine. The model is subjected to simple shear by applying relative displacements between opposite faces of the element at different velocities. . . . .	84
4.4	Validation of VUMAT time integration with an analytical model obtained by applying the Laplace-Carson transform to longitudinal and transverse shear tests at constant velocities of 0.006, 0.012, 0.024 mm/min. . . . .	85
4.5	Numerical Model of the $[\pm 45]_{2s}$ specimen . . . . .	86
4.6	a) Impact of strain rate on the viscoelastic material in the numerical specimen when the VUMAT routine is utilised. b) Comparison between the Numerical Results obtained with Abaqus using the VUMAT and the experiments on the specimen $[\pm 45]_{2s}$ . . . . .	86
4.7	a) Geometry of the two rubbing surfaces, b) Sketch of the pressure distribution during sliding. . . . .	87
4.8	Comparisons between the analytical model and experimental results for the Stribeck curves for the friction coefficient: a) Prepreg-prepreg contact, b) Prepreg-tool contact. . . . .	88
4.9	Model sensitivity analysis: a) Effect of wavelength $L$ variation keeping a constant roughness $A$ , b) schematic illustration of the wavelength changing. In c) is the effect of the roughness variation keeping constant wavelength $L$ , in d) is the schematic illustration of Amplitude changing. . . . .	89
4.10	Interlayer resin thickness, predicted with the developed model, as a function of the Hersey number. . . . .	90
4.11	Representation of thermoforming geometry . . . . .	91
4.12	Example of the mesh used in the simulation of thermoforming process . . . . .	92
4.13	Experimental thermoforming production process of prepreg with wrinkle formation	93
4.14	Simulation results of thermoforming process for the 4 layer laminate . . . . .	93

4.15	Evolution in the time of the simulation of the thermoforming process for the 32-layer laminate. . . . .	94
4.16	A comparison between the results of the numerical model of a 32-layer thermoformed prepreg and a real manufactured product . . . . .	94



# List of Tables

- 3.1 Uncured AS4/8552 0° Tensile Modulus for samples tested at a displacement rate of 1 *mm/min* at three different temperatures. . . . . 50
- 3.2 Average value and Standard deviation of friction coefficient for the ply-ply and ply-tool contact. . . . . 61
- 3.3 AS4/8552 Roughness *Ra* in  $\mu\text{m}$  for samples tested at 0.5 bar and pulled out at a displacement rate of 1 *mm/min*. . . . . 63
- 3.4 Thickness reduction and fibre bed equation for different laminates and temperatures. . . . . 69



# Chapter 1

## Synopsis of Composite Materials and Manufacturing Methods

Composite materials are complex materials comprised of two or more elements with very dissimilar physical or chemical characteristics. Smart mixes of different elements can provide the composite with the appropriate reaction, making it ideal for a particular application. Typical composites include cement, wood, and mud bricks, whereas more sophisticated composites are plastic/metal matrices reinforced with various types of fibres. These composite materials usually display anisotropy, which indicates that their properties change dramatically when evaluated in different directions. Typically, this occurs because the harder and stiffer component is in fibrous form with the fibre axes oriented in a certain direction, whereas the other component may exhibit inherent anisotropy due to their crystal structure.

The path of the history of fibrous composites begins with Owens Corning's discovery of Fibreglass in 1935 and Pierre Castan patenting Epoxy Resin in 1938; its rapid deployment to various military components during World War II was due to the exceptional weight-to-strength ratio. After initially recognising composites for their lightweight and robust properties, engineers quickly found alternative uses for them. Due to the material's radio frequency transparency, fibreglass composites were quickly adopted for use in shielding electronic radar systems (Radomes). After the discovery of continuous glassfibre, the next two decades (the 1940s and 1960s) were a time of boundless innovation in the fields of engineering and manufacturing; new materials such as Glass Fibre Reinforced Plastics (GFRP), phenolic composites, and sandwich-type structures were developed, and new manufacturing processes such as fibre winding, pultrusion, and wet lay-up mix with moulding systems were developed. The market took to this novel material right away, especially in the aviation sector (de Bruyne, 1937), but it also made waves in the automobile (Mangino et al., 2007), marine (Mouritz et al., 2001), and sports (J. L. Wang, 2012) sectors.

## 1.1 The Reinforcement Fibres

New innovations involving the use of composite materials were prompted by the aircraft industry's desire for lighter, stronger, and stiffer construction materials to replace aluminium and stressed plywood. Rapidly, new structural components were designed and incorporated into new aircraft types, such as the first glass fibre composite fuselage placed on the US Air Force's BT-15 aircraft (Figure 1.1a) and the FGRP wings put on the US training aircraft AT-6 (Figure 1.1b). These innovations were not commercially successful since the rigidity of glass fibre composites was insufficient, and weight savings relative to aluminum were minor. In addition, both the production methods and material characterisation were in their infancy. The manufacturing of basic structures constructed of glass fibre steadily decreased, and it was only present in components requiring frequency-dependent transparency, such as the radome of an airplane.



(a) US Air Force's BT-15



(b) US training aircraft AT-6

**Figure 1.1:** First aeroplanes to use glass fibre composite. Copyright information:

With the development of carbon fibres, the following decades (late 1950s and 1960s) marked a turning moment in the history of composite materials. Roger Bacon Bacon, 1960 published one of the earliest articles on carbon filaments in 1960, when he was able to produce carbon whiskers with a Young modulus of 700 GPa and a strength of 20,000 MPa, a material with a unique combination of stiffness, strength, and lightness. The cost of manufacture for carbon filaments was expensive at this time, but additional efforts helped to lower the costs while also improving the mechanical qualities of the filaments (Ford and Mitchell, 1963; Newcomb, 2016; Shindo, 1964). As was the case with glass fibre, increasing application, studies, and experience of their use led to rapid implementation of carbon fibres in a wide range of industries. This was accomplished by combining carbon fibres with plastic resins (both thermoset and thermoplastic), which resulted in the development of carbon fibre reinforced plastics (CFRP). Once the optimal combinations of fibre-to-resin volume were achieved, CFRP reached improved mechanical properties that allowed it to displace the conventional aeronautical materials like aluminium and titanium alloys that were present in primary and secondary aircraft structures (Soutis, 2005). The utilisation of composite materials in aircraft used by the military has been reignited, thanks in part to the participation of research institutes. The carbon fibre reinforced plastic (CFRP) is present in the wing tips of the Northrop F5 (Figure 1.2a) and the speed brake of the McDonnell F15 (Figure 1.2b). CFRP was the most popular kind of composite material utilised at this time. With the development of new aircraft, composite materials were

utilised in an increased number of structural sections. These composite materials accounted up 13% of the overall weight and were used in the rudders, and the skins of many other parts. CFRP had a similar role on civil aircraft, including the spoilers of the Boeing 737, Lockheed L-1001 fairing panels, and the rudders of the Douglas Aircraft DC-10. Elevators and horizontal stabilisers were Boeing's first principal structural installations on the B727 and B737. Lockheed then made a vertical stabiliser for the DC-10. In the early 1980s, carbon composite fairings were added to the Airbus 300, and spoilers, rudders, and airbrakes were added to the A310. These parts made up about 6% of the total weight of the structure. Beech and Piaggio made the first attempts to construct an all-composite aircraft in 1986 with the Starship and the P180 Avanti, respectively. In the same decade, the first composite helicopters were introduced: the Bell helicopter A-6E and the Bell-Boeing V22, both of which included 41% by weight composites. To the recent times, the composite composition in modern aircrafts like the Boeing 787 (Figure 1.2c) and the Airbus 350 (Figure 1.2d) represents more than 50% of the overall weight of these aircraft, making them contemporary icons on the use of composite materials in aeronautics and outstanding instances of the rising usage of (carbon fibre) composites.



(a) Northrop F-5 Freedom Fighter



(b) McDonnell Douglas F-15E Strike Eagle



(c) Boeing 787-9 Dreamliner



(d) Airbus A350-941

**Figure 1.2:** The aircrafts in (a) and (b) were the first to incorporate CFRP in their construction, accounting for 13% of the overall weight, whereas (c) and (d) are more recent models with a structural composite content of 55%. *Copyright ©: a) Guilherme Irber, b) Charles Cunliffe, c) Mark Van der Vliet and d) Vyacheslav Firsov.*

## 1.2 The Matrices

The incorporation of composite materials into industry and the subsequent revolution would not have been possible without the innovation and appearance of novel manufacturing techniques and material formulations. In addition to the advances in fibre technology, it is notable to highlight the advancements in resins used as matrices in composite materials. Nowadays, we can divide composites into two categories based on the type of resin used in their composition: Thermoset (Falzon and Pierce, 2020) and Thermoplastics (Vaidya, 2015). The most common type of polymer matrix composites (PMC) are thermosetting composites, mainly formed of free-flowing liquid or soft-tacky-solid macromolecules before processing. The composite material is subsequently solidified through polymer cross-linking, often at high temperatures and pressures and occasionally with the aid of a chemical catalyst. Epoxy resins have dominated the market for thermoset composites used in commercial aircraft constructions for the past 30–40 years because of its adaptability in design, ease of cure using a wide variety of initiators and curing agents, and moderate cure temperatures (Hamerton and Mooring, 2012). Engineers feel at ease with the idea of creating important structures from these materials because of the familiarity with their structure-property correlations.

PMR polyimides are another type of thermoset used in aeronautics. They were created by the US Air Force at NASA Langley to meet the operating requirement of 242–342 °C. This lets them be used in aircraft engine nozzles and nacelles, helicopter gear cases, and missile fins (Fernberg et al., 2018). Phenolic resins, another thermoset that contributes to some aircraft structures, were the major protagonists in the early attempts to use composites in aeronautics; however, these days, their use is limited to secondary structures like interior panels, flooring, and partitions, and even then, it is always employed with a modified chemistry (Asim et al., 2018; Xu et al., 2019). Commercially available cyanate esters are also used in aerospace, notably in radome applications. As a result of its higher thermo-mechanical and hot/wet performance compared to epoxy resins, it provides excellent cost and performance competence. It may be made into a potent thermal polymer by being strengthened and co-reacting with epoxy resins (Goyal and Cochran, 2022). Furthermore, polybenzoxazines are newcomers to the field of high performance resins, which are often combined with a second component, such as epoxy, to provide greater thermo/oxidative and hot/wet capacity to ordinary epoxies and cyanate esters. Their use in aircraft is restricted to interior panels, flooring, and partitions (Kiskan et al., 2011).

The development of thermoplastics has been analogous to that of thermosets, beginning with an experimental phase and then moving on to the production of entire components using thermoplastic. At this point in time, they are not extensively employed yet due to several concerns connected not to the practicability of the parts, but rather to the cost-effectiveness of the production procedures. The earliest application of thermoplastics on aircraft is observed in the US military’s F-22 jet fighter’s landing gear and weapons-bay doors in 1980, scaling up to current aircraft, the Airbus A380 with thermoplastic main wing leading edges and the Gulfstream Aerospace G650’s rudder and elevators. Utilizing thermoplastics as opposed to thermoset is primarily motivated by their thermoformability and weldability, which enables the manufacturing of structural composite components out-of-autoclave. This means significant savings in cost because thermoplastics are completely reacted and do not require

any reaction during cure. The long curing cycles of standard thermoset resin systems can be avoided, and a thermoplastic component can be consolidated in minutes, making the process simpler and faster (Offringa, 1996). Experience demonstrates that adapting the contemporary manufacturing process to thermoplastics is unaffordable due to the fact that processing temperatures are significantly greater compared to ordinary thermosets and the requisite equipments are more sophisticated, costly, and need process tooling with a low Coefficient of Thermal Expansion (CTE) (Bhudolia et al., 2020; Daso, 2019). Many attempts to obtain thermoplastic components by Automated Tape Laying (ATL) or Automated Fibre Placement (AFP) result in a poorly made and refined product. Polyetheretherketone (PEEK) is one of the most important thermoplastic resins used for structural purposes in the aerospace industry mainly to its lower melting point compared to other compounds of the same family, such as Polyetherketone (PEK) and Polyetherketonketone (PEKK) (Denault and Dumouchel, 1998). PEEK is already utilised in several aeroplane components, including the radome, fasteners, and even propellers (Berry, 2002; Shekar et al., 2009). The semicrystalline polymer PEKK has recently emerged for a broader range of applications than PEEK, including the potential fabrication of aeronautical primary structures using Continuous Compression Molding and In Situ Consolidation (Tadini et al., 2017). Manufacturing improvements that lower the cost of part production and simplify using thermoplastics in the aerospace sector would be a significant help in spreading their benefits.

In general, all types of composites currently available on the market are being used in various industrial sectors, replacing traditional materials such as aluminium, titanium, and metallic alloys; changing the worldwide market in an effort to find materials with improved mechanical performance and lower prices. By 2021, the composite market had regained its pre-pandemic growth rates and attained an expected output value of more than \$100 billion and a volume over 12 million tonnes (Mt). Being thermoset resins used more frequently (60%) than thermoplastic resins (40%) and glass fibres being the most commonly used reinforcement (88%), as opposed to natural fibres (11%) and carbon fibre (1%). Composite materials are present in virtually all regions of the world and all application sectors, with China and the United States being the largest consumer markets. The new generation of automobiles will be one of the key growth factors and additive manufacturing (Holmes, 2019) will be the innovative method that drives the composites industry to greater heights (Eric Pierrejean, 2022; Koumoulos et al., 2019).

### 1.3 Manufacturing Methods for Polymer Matrix Composites

Along with efforts to improve aeronautical materials, important progress may be made on developing new methods for building aircraft structures. The evolution of how composite materials are made is a vast topic due to the many different ways to combine composites, applications, and strategies to automate the processes. There are a plenty of reviews about composite manufacturing available in literature that go into more details on this subject like Chohan et al., 2020; Li et al., 2022; Mesogitis et al., 2014; Qiao et al., 2022; Rajak et al., 2019; Talreja, 2019. As a general rule, these four basic steps are necessary to create a PMC

structural part of any kind:

- Impregnation
- Lay-up
- Consolidation
- Solidification

These procedures are fundamental to any way of producing composites (Buragohain, 2017). However, the manufacturing technique and physical shape of the reinforcement and matrix determine the specific sequence in which these operations are carried out. In the impregnation process, the fibres are wet with resin. A correct wetting is required to prevent discontinuities in the resin distribution that contribute to composite failure (Gibson and Manson, 1992). Different fibre/resin volume fractions may be matched depending on the component's purpose, and these ratios can be adjusted more significantly by the resin state. In addition to the surface tension and capillary action, the viscosity of the resin is a critical feature that influences the impregnation of the fibre (Hamidi and Altan, 2017). Impregnation is performed throughout the manufacturing process for all wet lay-up and wet winding techniques. In wet filament winding, for instance, the fibres are soaked in a resin solution before being deposited on the mandrel. In a similar manner, cloth plies are put on a mould and wetted with resin using an application brush in wet hand lay-up. Alternatively, in the dry lay-up and dry winding procedures, reinforcements are impregnated during prepreg/towpreg production. The structural performance of a composite item is highly dependent on the conforming ply sequence; hence, lay-up is a manufacturing phase that requires careful attention (Ghiasi et al., 2010). When using fabric plies, this stacking is done by placing a certain number of plies in a specific direction along the length of the fibres. When winding filaments, on the other hand, the mandrel and carriage unit's respective movements are controlled by winding programmes. In the composites manufacturing process, excessive resin and trapped air are eliminated using a procedure called consolidation (Kratz et al., 2021). To achieve a high quality composite, close contact between the laminae must be established. When using a roller in a hand lay-up operation, excessive resin is removed. Also, it is common practise to apply pressure for consolidation purposes throughout the curing process. Consolidation and lay-up occur concurrently in procedures like filament winding because the tension created by winding the rovings provides enough consolidation pressure. Solidification is often the last phase of the process, and its primary function is to give the composite component a physical solid form. During this step, the resin is allowed to cure, at which point the process of cross-linking will take place, and the resin will begin to solidify. The curing cycle, as well as the necessary conditions of positive pressure, vacuum, and temperature, will be primarily determined by the cure kinetics of the resin that is selected (Muc et al., 2019).

This four fundamental step are generally featured in all the manufacturing processes developed for composite part production. The steps do not have to be executed in the same sequence as shown below, and in many instances, more than one step is performed concurrently. Figure 1.3 illustrates a summary of all composite manufacturing techniques known until today and used in various sectors, organised by the type of resin involved. This diagram demonstrates the connection between the kind of resin, the type of fibre, and the manufacturing process that

could combine the two materials into a composite component. Some of the most significant manufacturing processes used in the aeronautics sector are briefly described below.

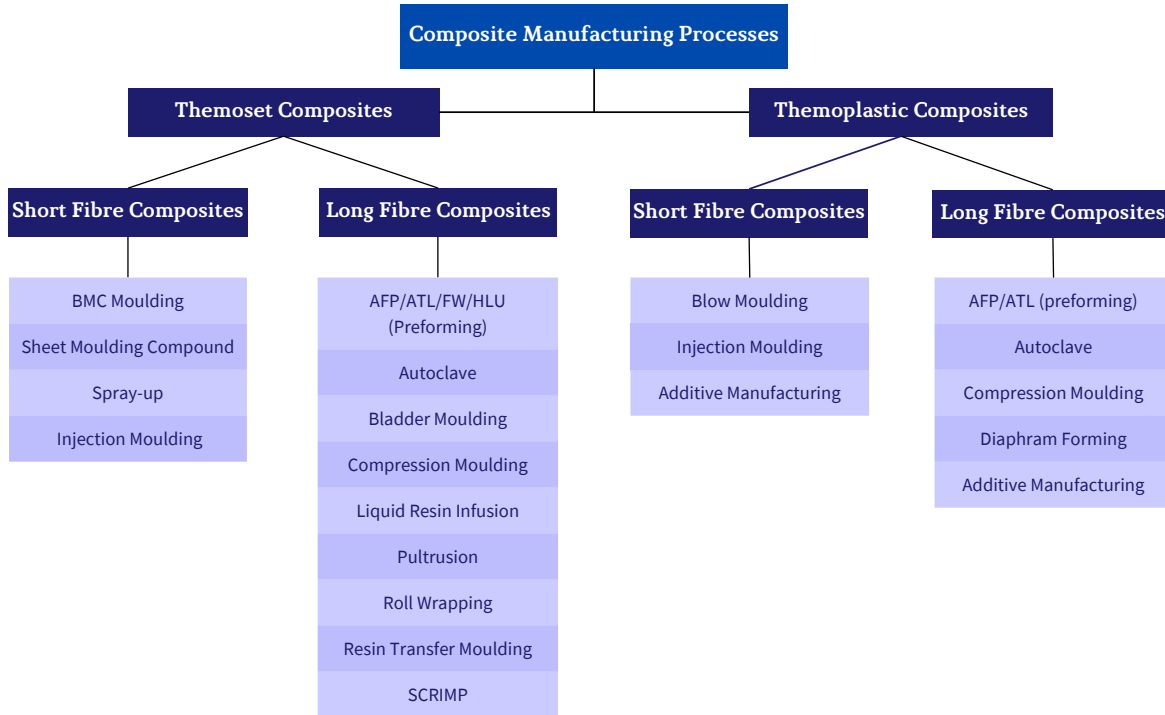


**Figure 1.3:** An synopsis of all composite manufacturing processes organised by the kind of resin and fibre used (Pantelakis, 2020).

### 1.3.1 Injection Moulding

Injection moulding is a popular polymer manufacturing technique used to create a variety of plastic composite products. The process typically involves the use of a reciprocating single-screw extrusion machine to transport, melt, and pressurize granular fibre-filled polymeric ingredients supplied into the machine. As the polymer melt is sheared inside the machine, heat conduction through the barrel wall and heat dissipation causes the polymer to melt within the barrel. During plasticisation, the polymer melt builds up in front of the screw, which is then forced back against an adjustable pressure inside the hydraulic system until the desired shot size is achieved. Once the shot size is attained, the screw pulls forward to drive the polymer melt through a runner system and into the relatively cool, empty chamber of the previously closed mould. To compensate for any shrinkage induced by the cooling of the melt inside the cavity, the melt in front of the screw is retained under pressure, allowing additional material to be forced into the cavity. As the material is supplied through the gate into the mould, water runs through channels to maintain the mould cavity walls at a temperature between the ambient temperature and the polymeric materials' glass transition temperature (for amorphous polymers) or melt temperature (for semi-crystalline polymers).

Once the material has filled the cavity and solidified, the mould opens, and the finished product is ejected (S.-J. Liu, 2012). There are certain limitations to the process, such as a limit on the length of the fibres used, which can affect the composite's performance. Short fibre lengths lead to an increase in fibre volume and therefore an increase in composite quality (Balasubramanian et al., 2018).

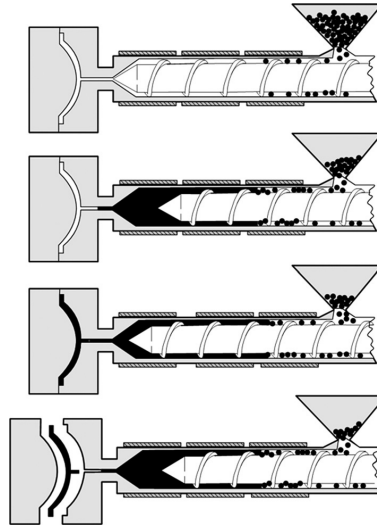


**Figure 1.4:** Illustration of Injection Moulding

### 1.3.2 Resin Transfer Moulding (RTM)

Resin Transfer Moulding (RTM) (Hsiao and Heider, 2012) is a composite manufacturing technology used to produce lightweight, high-performance structures. A liquid resin, often epoxy, is injected into a closed mould containing reinforcing fibres, such as carbon, glass, or aramid fibres. The resin infiltrates the fibres, causing a chemical reaction that cures the resin and bonds the fibres together, resulting in a composite structure that is solid, strong, and lightweight. The aerospace industry has employed composite materials for decades, but the RTM technique has gained popularity because to its efficacy and flexibility for producing tiny to medium-sized structural components in low to medium-volume manufacturing. The use of RTM in aerospace applications has also resulted to substantial advancements in aircraft design, enabling the production of components that are both aerodynamically efficient and structurally robust. Even so, to ensure appropriate resin flow, void-free and dry fiber-free components, a complex tooling design is required, which might be viewed as a drawback considering that it requires several tries to get an ideal process.

### 1.3.3 Filament Winding (FW)

During filament winding, rovings are placed around a mandrel in specific patterns. So that the fibres are laid down in a homogeneous pattern on the mandrel surface and the desired thickness and ply orientation are achieved, winding programmes are utilised (Henriquez and Mertiny, 2018). Once the newly applied composite on the mandrel has hardened, the mandrel may be taken out, revealing the component. It is interesting to observe how the four essential

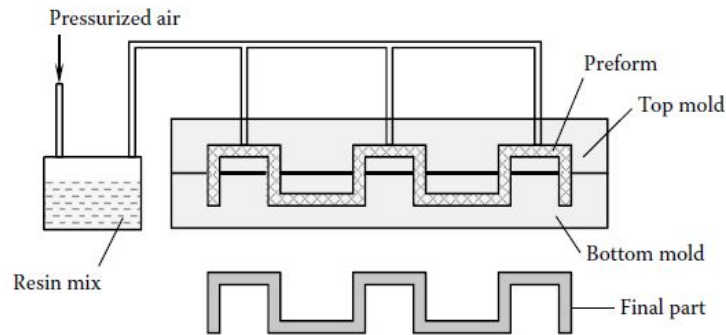


**Figure 1.5:** Simplified RTM system for manufacture of composite components

processes of composites manufacturing are combined into the filament winding process. There are three distinct approaches to the impregnation phase: wet, wet rolled, and dry. Dry tows of fibres are immersed in a resin bath before being placed on a revolving mandrel, which is the essence of the wet impregnation process. In the second and third cases, the mandrel is used to wind wet rolled fibres or prepreg tows (towpregs). Dry rovings are rerolled after being wetted with a measured amount of resin to create wet rolled rovings, which are then used for winding. Either they are put to use immediately after being respooled, or they are frozen for later use. Dry winding is the term used to describe the process of winding using fibres that have not been wetted at any point in the winding operation, such as when using wet rolled rovings or towpregs. It's a clean manufacturing procedure that guarantees consistency in the cured part's fibre volume fraction. A fiber-depositing mechanism known as pay-out-eye deposits the wetted rovings onto the rotating mandrel. A winding programme controls the rotation of the mandrel, the motions of the carriage unit and the pay-out eye, and the relative motions of the carriage unit and the mandrel result in the desired route along which the fibres are deposited. The ply orientation angle is the angle of winding along the fibre route on the mandrel surface. To maintain the rovings straight between the pay-out eye and the fibre touch-down point on the mandrel, tension is applied to them during filament winding. In addition, tension is generated as the rovings are drawn into the resin bath and directed through the roller system. A component of the wandering tension operates in the inward normal direction, producing a consolidation pressure. Thus, consolidation occurs during the actual winding process.

### 1.3.4 Additive Manufacturing

Additive manufacturing (AM), often known as 3D printing, is a process of adding materials to construct products using three-dimensional (3D) models (CAD models) in consecutive layers, as opposed to traditional subtractive manufacturing processes. Over the course of more than two decades, several unique AM techniques with applications in aerospace, automotive, biomedical, digital art, architectural design, etc. have been created. The process of 3D printing using composite materials includes creating a 3D model, slicing it into layers, producing a mixture of matrix and reinforcing materials, printing the item layer by layer, and curing it with heat or light. The reinforcing material supplies the matrix material with strength and

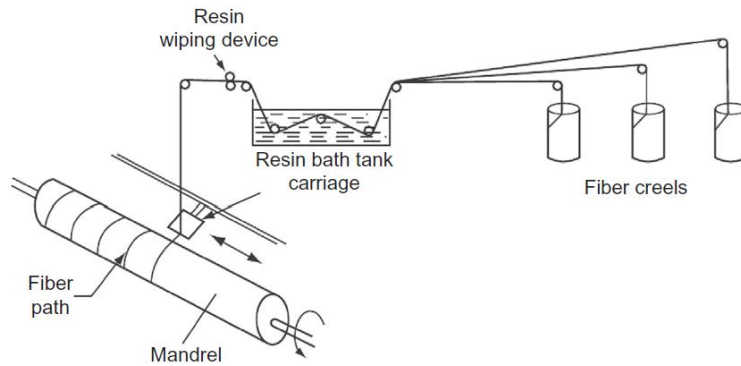


**Figure 1.6:** An illustration of the winding of a filament (Mallick, 2007).

stiffness, resulting in objects with customizable mechanical characteristics (Velu et al., 2019). Fiber reinforcement may significantly improve the mechanical characteristics of 3D-printed polymer matrix pieces but continuous fibre reinforcement is now one of the greatest obstacles in 3D printing polymer composites. It provides a considerable increase in mechanical qualities compared to discontinuous fibres, but no consistent and standard paradigm for 3D printing continuous fibre composites has yet been devised (Parandoush and Lin, 2017).

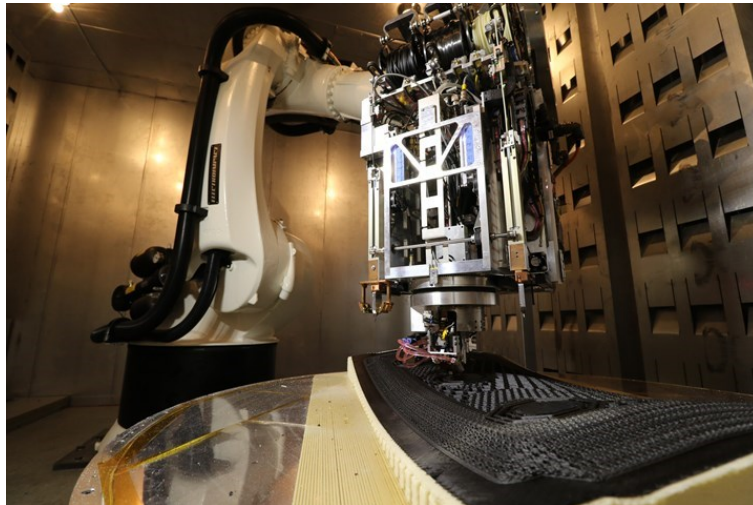


**Figure 1.7:** Example of the concurrent use of composites manufacturing and additive manufacturing.  
*Copyright ©Electroimpact.*

## 1.4 Preimpregnated composites and its applications in aerospace engineering.

A preimpregnated composite is defined in the group of composite materials as a reinforcing fabric that has been preimpregnated in a resin system (usually thermoset Epoxy) that already includes an appropriate curing agent. This action let the material in a state known as "B-stage" and can be stored for a limited period at low temperature and can be used on a later date

(Buragohain, 2017). This form of composite is commonly referred to as "Prepreg," and it will be referred to in this manner throughout the rest of the monograph. Prepregs are meant to solve one of the most difficult parts of composites manufacturing: resin impregnation of reinforcement, which becomes more problematic as resin viscosity increases. Imperfect impregnation results in dried fibres and entrapped air, which leaves voids in the finished product and affects its mechanical qualities (Hassan, 2021). Depending on the reinforcing type, resin matrix, and intended purpose, a variety of formats are possible. Commercially available products are made up of unsaturated polyester, epoxy, phenolic, and thermoplastics reinforced with glass, carbon, and aramid being the unidirectionally reinforced prepregs more frequent than fabric-based alternatives. The layers of prepreg are ready to be stacked and moulded in a system that combines pressure and heat in order to produce a structure component. During the production of prepreg composite parts, this B-staged prepreg must be heated in an autoclave or oven to accomplish complete polymerisation. Prepreg composites meet the high-performance, lightweight, strength, and durability requirements of an aircraft structure. They have been utilised in the aerospace industry since the 1960s, with the Apollo Lunar Module using prepreg landing gear struts, engine heat shields, and other important components. Their good performance in the Lunar Module established the potential of prepreg composites for aerospace applications, making way for wider aerospace industry adoption. Throughout the 1970s and 1980s, the utilisation of prepreg composites in the aerospace sector increased, but producing a chronological analysis on the technical growth of the prepreg material and the manufacturing procedures employing prepreg composite is difficult owing to the fact that these advancements are selectively published due to intellectual property rights, and many specifics are often protected. Prepreg composites are now often employed in the aerospace sector for a wide range of applications, such as the construction of aeroplane wings, fuselages, and engine parts (Pantelakis, 2020). In order to meet the strict requirements of contemporary aerospace applications, new resin systems and reinforcement materials have been developed throughout time as well as new manufacturing procedures.

There are several manufacturing methods that can be used to build aircraft components with prepreg composites, but the most common methods used in the aerospace industry are autoclave curing and out-of-autoclave (OOA) curing. In both cases, the operation begins by stacking layers of prepreg on a tool to create a laminate with the desired shape. The laminate is then sealed in a vacuum bag assembly and either autoclaved or consolidated using an alternative method. Large aeroplane parts like wings and fuselage are increasingly being made with prepreg composite in autoclaves. Within this process, the temperature and pressure will allow the resin to flow and impregnate the fabric, reducing the fabric's porosity by pushing out surplus resin and collapsing trapped air bubbles as the laminate is formed. The equipment works as a subsequent stage on the part production, right after the impregnation and the lay-up and can process a broad range of materials, including thermoset and thermoplastic-based composite aircraft components with varied contours and complicated geometries (Ramaswamy Setty et al., 2011). Autoclave processing is well-understood, well-established, and serves as a baseline for competing techniques, but the size of the component to be manufactured restricts its usage since it is not cost-effective to consolidate small components in a big autoclave, and this delays and affects manufacturing efficiency as well (Shaik et al., 2021). As the demand for these FRP structures continues to rise, there is a growing need for novel ways that

are both quicker and more cost-effective. Numerous OOA approaches have been developed to satisfy these needs by providing more flexible manufacturing environments in order to produce secondary structures and even primary structures with a quality that is comparable to that of an autoclave (Centea et al., 2015). A new generation of out-of-autoclave prepregs has been produced, and experience with these prepregs has shown that vacuum bag-only (VBO) consolidation could be used to generate autoclave-quality components. In this regard, we may highlight various production methods that cover the impregnation and lay-up phases and can be integrated with autoclave equipment, as well as methods that can fully generate a component without the need for an autoclave. In the aerospace industry, hand lay-up, ATL, AFP, RTM, and thermoforming are the most prevalent techniques combined with autoclave that we can identify. For out-of-autoclave methods, we may mention Vacuum Assisted Prepreg Compression Moulding (VA-PCM), Filament Winding, and OOA Vacuum-Bag-Only (VBO) for prepregs (Ekuase et al., 2022).

Prepregs are manufactured with specialised equipment under tightly regulated conditions, resulting in a low void content and homogeneous fibre dispersion. The materials can be measured and combined to achieve consistent qualities with defined parameters. Generally, they result in greater quality and more homogeneous final goods. Two basic methods are used to create prepregs: the hot melt procedure and the solvent dip approach (“Technology update: Prepregs”, 2003).

- Hot Melt Process

The hot melt procedure is able to make both fabric and unidirectional prepregs simultaneously. This procedure can be broken down into two steps. In the initial step of the process, a substrate made of paper is covered with a very thin layer of heated resin, after which the fibres are soaked in the resin. In the prepreg machine, the reinforcing material and the resin are both given the opportunity to interact with one another and usually sandwiched with another carrier paper (dry or laminated). Sandwiched fibers are pulled through heated compaction rolls, and then lead through cooling rolls. In the final stage of the process, one of the carrier papers is removed and the final prepreg is rerolled with the one back-up paper.

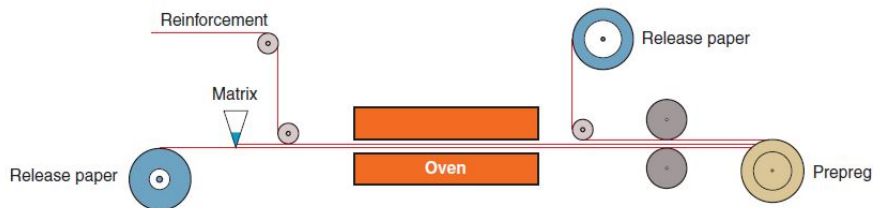


**Figure 1.8:** Hot Melt Process for prepreg production.

- Solvent Coating Process

In the process of solvent coating, the fabric is first fed into a resin solution while being threaded between metal rollers, and then it is passed through a succession of furnaces in order to partially cure the material. After undergoing a brief time of cooling, the prepreg is eventually wound up at the opposite end of the machine into a roll with

the purpose of making it more convenient to store. The viscosity of the resin in the bath is decreased by dissolving it in a solvent, which is commonly alcohol or acetone. This allows the resin to have a greater capacity to penetrate the fibres. As a part of the process that takes place during B-staging, the solvents are allowed to evaporate as volatiles in large in-line ovens.

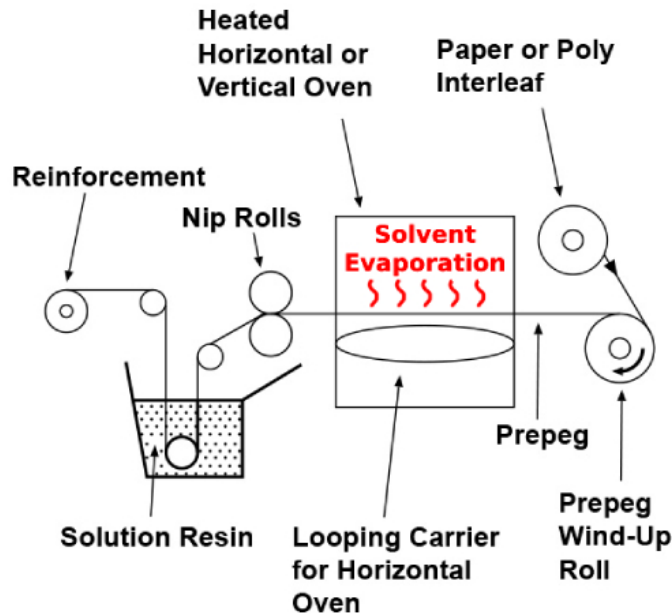


Figure 1.9: Solvent Dip Process for prepreg production.

## 1.5 Thermoforming manufacturing to produce thermoset prepreg composites

The simplicity that prepregs present stand them out from classic known techniques for composite part production due to certain advantages: The strength properties are enhanced since a more optimum fibre-resin proportion is achieved. By employing prepreg the resin volume can be easily achieved which is ideal for maximum cured properties. Prepregs reduce significantly the problems of dry spots and resin-rich zones, granting a uniform thickness and the parts come out of the mould with a theoretical likelihood of being identical. This is what in manufacturing is known as a good part uniformity and repeatability. In terms of efficiency, prepregs need less curing time, with the part ready for service after completing the heat curing cycle. The part production generates less mess and waste when compared to other manufacturing processes for composite components. The final result is a part structure with a superior surface finish on the exterior and less void content in the interior.

To manufacture a thermoset prepreg composite component for an aeronautic purpose, one would typically begin by stacking the prepreg plies using HLU, ATL, or AFP on a mould, consolidate the laminate using a thermoforming cycle assisted by vacuum, and finish solidifying the part in an autoclave. Below are outlined some of the common procedures for laying up prepreg plies.

- Hand Lay-up (HLU)

The hand lay-up method, often known as the wet method, is one of the most commonly used processes in composite manufacturing. This basic procedure consists of manually stacking layers to create the laminate (Figure 1.10). This stacking can be done with dry fibres that will be impregnated in a second phase or with preimpregnated plies. If dry fibres are taken into account, the entire manufacturing procedure will require an impregnation, consolidation, and solidification phase. If preimpregnated fibres are taken into account, only consolidation and solidification remain. The specific types of complementary stages used to meet the demands of the structure are open to the interpretation of the user. The approach is trustworthy, but it is not the most efficient because it is labor-intensive and time-consuming in comparison to more sophisticated procedures. This technology is intended for secondary components with basic geometries for aviation applications, while more complex components may require sophisticated production processes (Balasubramanian et al., 2018).

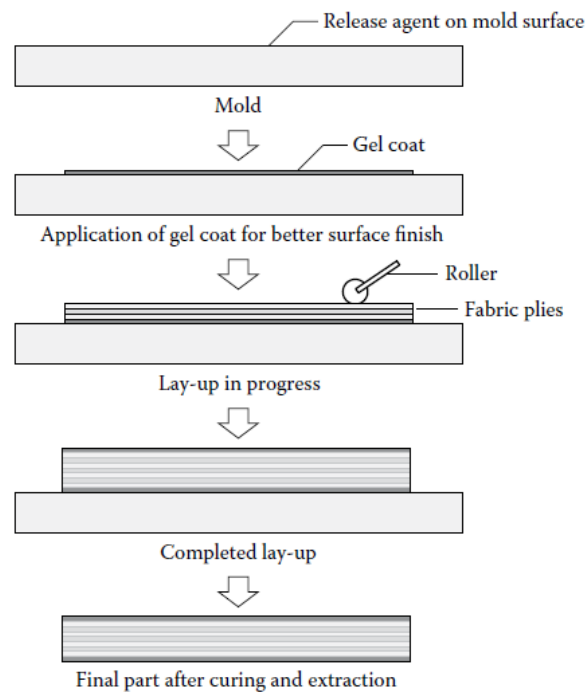


**Figure 1.10:** Illustration of the hand lay-up procedure (Buragohain, 2017).

- Automated Tape Laying (ATL) and Automated Fibre Placement (AFP)

Since the principles of these two approaches are identical, they are typically discussed together. They consist of a tape or fibre feeding system with a cutting mechanism that automatically deposits the material in the desired stacking order while compacting it with a roller over a flat surface or a mould (Figure 1.11). By automating the process, these technologies aim to boost the deposition ratio relative to hand lay-up. These enhancements are four times more efficient than manual lay-up, while simultaneously minimising material waste and attaining high reproducibility. ATL is quicker than

AFP if the component has minimally contoured surfaces, however, AFP is used if the part has complicated geometry with curved zones since it is more accurate for these requirements (Marsh, 2011). Both techniques are confined to the lay-up stage, although the impregnation gets involved since it is typically used with prepreg composites. There is still a need for a second period of consolidation and hardening.

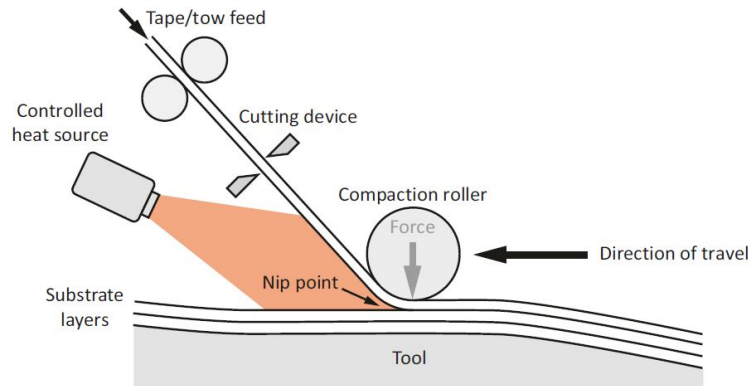


**Figure 1.11:** Diagram of a standard dispensing head for Automated Tape Laying (ATL) and Automated Fibre Placement (AFP) machines (Falzon and Pierce, 2020).

### 1.5.1 Thermoforming process

Thermoforming is a broad term for a process in which a material is heated to a temperature range where the material is more malleable, and then reshaped using a mould system that can regulate temperature, displacement velocity, and pressure. It is typically a consequence of the fibers placement. Although this technique has been around for quite some time and it was originally developed for cellulose nitrate, it didn't gain widespread use until the advent of the plastics industry in the 1930s. All types of plastic, including semi-crystalline, bio-based, foamed, filled, and reinforced, were quickly linked to it. Thermoforming was initially used in the aerospace industry to create plastic items like acrylic gun enclosures and windscreens in military aircrafts (P. Martin, 2009). Since the development of prepregs, thermoforming has evolved into one of the primary production processes for aerospace structures. Parts production via thermoforming is a perfect fit for the aerospace industry as it helps to reduce the time and effort spent on making composite structures while simultaneously raising the bar for quality and providing finished aircraft structural components in the quest for complex forms (Throne, 2011). A thermoforming process may have various variations depending on the technology utilised, such as hot-diaphragm, matched-mould procedures, autoclave systems, and so on (Garcia-Gil, 2003). Despite these differences, they all follow the same operation stages. In high-standard industrial manufacturing, prepreg composite plies are piled and put over heated surfaces or moulds utilising ATL or AFP equipment. A thermal cycle is then initiated, which should include a heating stage to allow the resin to gel and become more malleable. To avoid premature strains into the laminate and allow the plies to deposit over the hard mould, contact surfaces must stay unattached (J. P. Belnoue et al., 2017). Consolidation begins at a steady velocity and pressure, compacting the laminate to the required shape. The final stage is determined by the thermoforming technology used,

although it often involves using a vacuum pressure to apply a consistent force throughout the whole object and remove the entrapped air between the plies. Figure 1.12 shows a schematic of a thermoforming method that uses two matched moulds to consolidate the laminate and its corresponding thermal cycle.

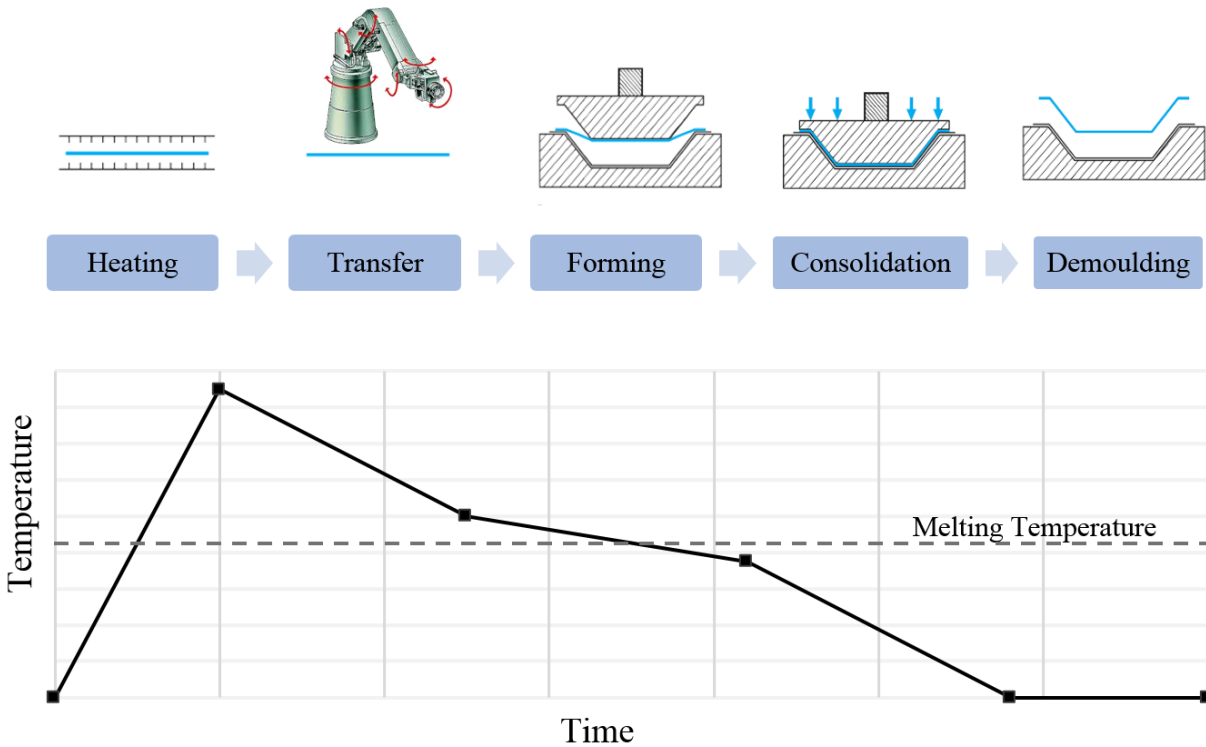


**Figure 1.12:** Thermoforming process of prepreg sheets including a thermal diagram (Guzman-Maldonado et al., 2016).

### 1.5.2 Thermoforming: Wrinkles and Defects

The thermoforming process includes the induction of normal and shear stresses into the ply laminate, as well as interlaminar shearing and bending forces across the entire laminate. Wrinkles and other imperfections in the finished structure might result from these loads mixed with the intricate geometry of the mould, the stacking sequence, and the production circumstances affecting the ultimate mechanical characteristics and durability of the product, resulting in a 40% reduction in strength (Boisse et al., 2011) (Figure 1.13). The mechanism that causes this unwanted fold is still a topic of debate, and it needs to be completely described in order to optimise the manufacturing process so that a perfect quality part with a faultless surface finish may be produced. Some authors in the literature classified wrinkling into two types: in-plane wrinkling and out-of-plane wrinkling (Hallander et al., 2015). The first scenario is less common and is generated by fibre waviness rather than uniform strain induced by load combinations or boundary circumstances (Guzman-Maldonado et al., 2015). Lightfoot et al., 2013 investigated the ply wrinkling mechanism caused by shear between plies and identified ply-tool and ply-ply shear as essential process parameters for defect generation. He notices that during the early stages of the temperature cycle during consolidation, the plies

might move relative to one another and to the mould, creating friction and shear stresses. These shear stresses fluctuate according to the mould geometry, altering the strain on the contact surfaces and causing wrinkle development. This instance has been analysed for various stacking sequences (Hallander et al., 2015), the influence of release films between the ply-tool contact surface (L. Wang et al., 2019), a double diaphragm with a C-shape (Sun et al., 2012), tool surface roughness (Mulvihill and Sutcliffe, 2017), and variable process condition factors (Pasco et al., 2019; Sun et al., 2014).

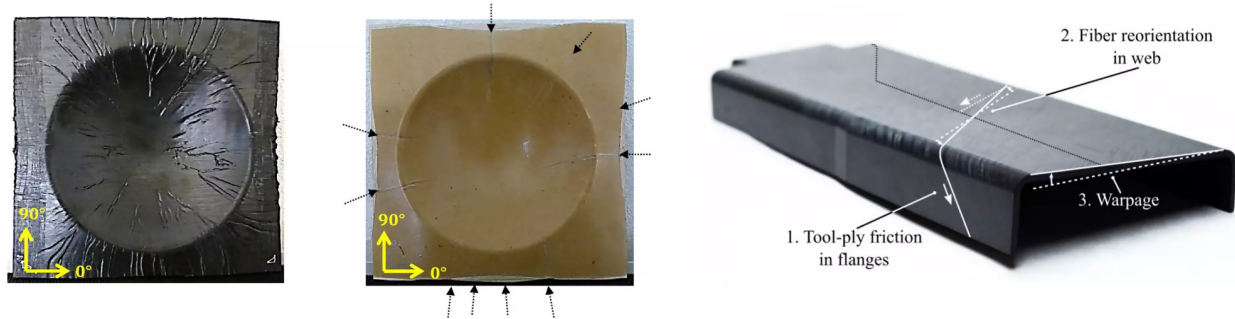


**Figure 1.13:** Regular wrinkles noticed during thermoforming of composite plies. These irregularities lead to undesired displacements, reorientation of the fibres, and warpage (Slange, 2019; Wolthuizen et al., 2014).

Shear between plies during forming and slippage between plies during consolidation are two mechanisms that can cause wrinkle flaws in composite production. As indicated in 1, friction resistance plays a crucial role in the creation of wrinkling defects for both wrinkle mechanisms: inter-ply shear (slippage), ply-tool contact, and ply-ply sliding, resulting in process-induced deformations and a reduction in part quality. Bending stiffness is another property that contributes to the formation of thermoforming flaws. This property, in particular, acts as a barrier to folding and, as a result, the development of wrinkling (Skordos et al., 2007). Due to the relative motion of the fibres, despite the in-plane rigidity of the textile, poor bending stiffness is predicted when compared to other rigid materials (sheet metal or composite plates) (Boisse et al., 2011). Several experimental approaches for estimating bending stiffness have been presented in the literature regarding prepreg material in thermoforming manufacturing. A collection of prepreg bending tests can be found in Ropers et al., 2016, with the most remarked on cantilever beam (Liang et al., 2014), Kawabata beam (Sachs, 2014), and V-bending tests (Uriya et al., 2014), as well as its modifications. Bending behaviour is independent of tensile and shear characteristics and so cannot be predicted using computed values. In numerical modelling, the estimated bending stiffness has several meanings, although it is typically regarded as a viscoelastic property. Dörr et al., 2017 modelled rate-dependent bending behaviour using a finite strain viscoelastic technique, a Kelvin-Voigt approach, and a generalised Maxwell approach, which were implemented in a commercial FE solver utilising both implicit and explicit time integration. The generalised Maxwell technique in combination with non-linear viscous behaviour is best suited for viscoelastic bending behaviour. Alshahrani and Hojjati, 2017 used AniForm software to create a FE model based on a Kelvin-Voigt method. They came to the conclusion that bending stiffness is highly dependent on the lay-up, which his model was able to simulate in most situations with some difficulty at particular stacking sequences. Guzman-Maldonado et al., 2019 provide another numerical analysis

based on a simplified version of the virtual work concept, defining virtual work in a virtual displacement field as the total of virtual work owing to tension, in-plane shear, and bending. The majority of the authors cited concluded that friction resistance and bending stiffness are important parameters in wrinkling generation and must be thoroughly characterised.

## 1.6 Aims and scopes

Thermoforming is a vital production method in the aerospace sector, where thermoset composite materials are employed widely owing to their lightweight and high-strength features. However, the thermoforming process is affected by defects such as wrinkling, which may damage the integrity of the finished product. Exploring thermoforming manufacturing defects and the mechanical response of uncured thermoset prepreg materials is fundamental since it offers the possibility for considerable improvements in production processes. The present thermoforming manufacturing procedures are based on trial and error, resulting in higher production times and costs. By providing a reliable and extensive mechanical characterisation of the uncured thermoset prepreg composite material upon which numerical models can be established, this project will enable the industry to make more informed decisions, thereby reducing manufacturing time and costs and improving the quality of the final product.

The primary objective of this study is to investigate the mechanical performance of the uncured AS4/8552 thermoset composite subjected to thermoforming process conditions (namely temperatures of 40°C and 60°C, that are pertinent to aviation applications). This material is a commonly used thermoset prepreg composite in the aerospace sector, and the outcomes defined in this research will have a substantial influence on its production process. To accomplish this purpose, a thorough material characterisation must be undertaken, which includes in-plane and out-of-plane property calculations for a laminate. This characterisation will provide a full knowledge of the material's characteristics, allowing for the creation of precise numerical models that may be used in actual thermoforming manufacturing operations.

The research will also conduct experimental analyses of various thermoforming-related phenomena, including interply friction resistance, bending stiffness, fibre bed effect, and resin bleeding effect. These processes are crucial to the thermoforming process and significantly affect the quality of the final product. The study will build a more thorough knowledge of the thermoforming process by investigating these processes, and supplying more precise material parameters to feed numerical models.

# Chapter 2

## Materials and experimental techniques for the mechanical characterisation of uncured prepregs

The present chapter provides an extended description of the selected prepreg composite material and a comprehensive review of standard methods for the mechanical assessment of fibre-reinforced composite materials (FRC) as documented in the literature. Subsequently, an in-depth examination of the implementation of these techniques for uncured prepreg laminated composites is presented because the standard methods designed for cured laminates yielded inconsistent results. The diagram illustrated in Figure 2.1 outlines the preliminary conceptual framework devoted to capturing the material behaviour at different stages, including the characterisation of plies at the mesoscale, often known as intraply behaviour and the analysis of the interaction between plies or interply behaviour.

### 2.1 Material

AS4/8552 UD carbon fibres pre-impregnated sheets manufactured by Hexcel with a nominal uncured ply thickness of 0.221 mm and fibre volume fraction of 57% were selected for this investigation because of their extensive use in the aerospace sector, primarily for the thermoforming fabrication of primary structures. HexTow AS4 carbon fibres, which are continuous, high strength, high strain, and Polyacrylonitrile (PAN) based, are incorporated into this prepreg. The fibres have been surface-treated and may be sized to increase their interlaminar shear qualities, handling characteristics, and structural properties, allowing them to be employed with various techniques, including weaving, prepregging, filament winding, braiding, and pultrusion. About the resin, HexPly 8552 strong epoxy matrix is recommended due to its high performance for use in major aircraft constructions. It has strong impact resistance and damage tolerance for various applications. The primary characteristics of the uncured prepregs are the excellent tack and controlled matrix flow during processing. After curing, the glass transition temperature of 154°C makes it possible to obtain good mechanical properties of the laminates up to 120°C. However, in its uncured form, the material exhibits

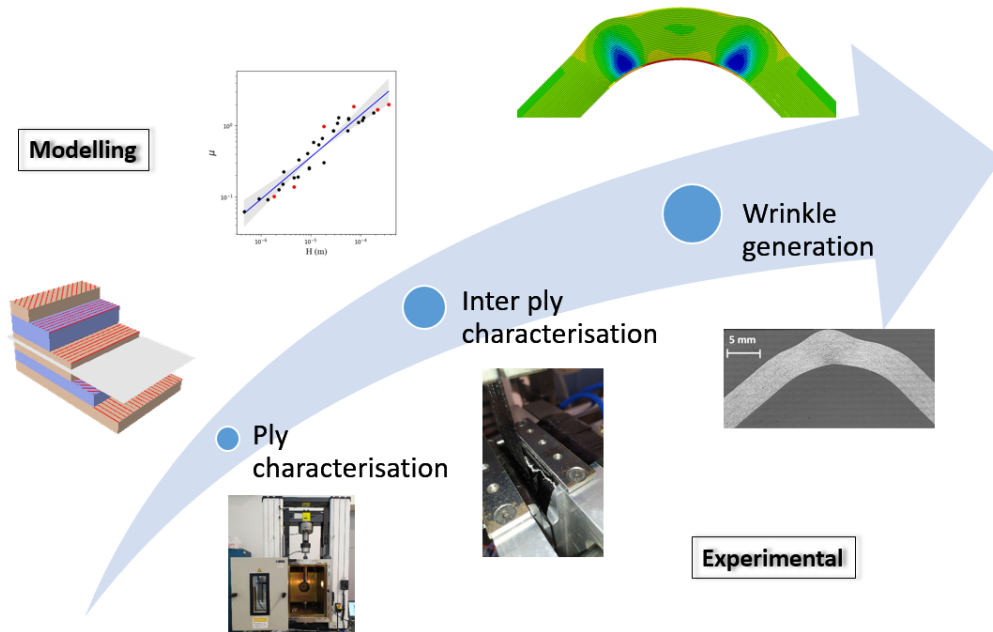


**Figure 2.1:** Characterisation method

a strong viscoelastic response for those matrix-dominated properties (e.g. transverse to the fibres, shear). Significant non-linear deformations attributed to the soft matrix behaviour and relatively facile sliding between the plies of the uncured laminates prevent standardised methods for material characterisation.

## 2.2 Mechanical characterisation of cured prepreg laminates

The mechanical behaviour of a specific type of material is frequently the first task to perform when a new design application is planned. Even though these unitary features will not be the ultimate deciding factor in the overall design, they serve as a benchmark for the decision-making process. The difficulty of successfully executing an experimental characterisation of a material increases with its complexity. In particular, it is well known that composite materials exhibit anisotropic behaviour induced by the presence of fibre architecture. Since a fibre-reinforced lamina is an orthotropic material with transversely isotropic symmetry, it has a higher ratio of axial stiffness to transverse stiffness and longitudinal shear than other materials. For this reason, the mechanical characterisation of a unidirectional lamina (UD) is one of the most challenging problems compared to other composites (Saba et al., 2019). The test's progress can also be affected by how the material is composed and how the composite constituents are distributed, creating a disparity of non-linear behaviour and complex failure modes (Duvaut et al., 2000). An individual lamina is the primary unit or building component for most fibre-reinforced polymers (FRP). Whether the lamina is UD prepreg, a fabric, a chopped-strand mat, or another fibre form, the characteristics of the individual laminae must be determined for design purposes. The possibility of creating a laminate by stacking

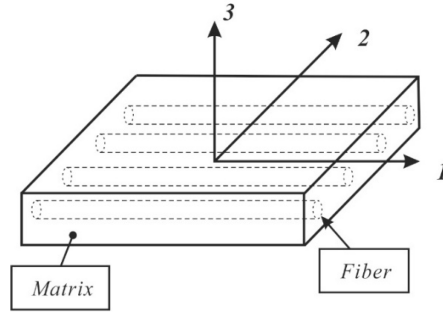


**Figure 2.2:** Material axis for fiber-reinforced composite ply schematic (Chen et al., 2018).

individual plies following a given sequence makes possible various experimental designs. When the classical lamination theory (CLT) supports these analyses, they can lead to the discovery of the primary lamina characteristics. Let us assume a ply as an orthotropic elastic solid in which the orientation axis is formed as follows: direction 1 (longitudinal direction), direction 2 (in-plane), and direction 3 (through-the-thickness) as shown in Figure 2.2.

Then, the five mechanical constants referred to such material orientation system will be Young's modulus in the fibre direction ( $E_{11}$ ), Young's modulus in the perpendicular-to-the-fibre direction ( $E_{22}$ ), the in-plane shear modulus ( $G_{12}$ ), and the in-plane Poisson's ratio ( $\nu_{12}$ ). Furthermore, using the plane 2-3 as the material plane of symmetry for transversely isotropic materials, the following relations may be accepted in a statistical sense:  $E_{22} = E_{33}$ ,  $G_{12} = G_{13}$ , and  $G_{23} = E_{22}/2(1 + \nu_{23})$ . Under these conditions, the constitutive equation stays as follows:

$$\begin{Bmatrix} \epsilon_{11} \\ \epsilon_{22} \\ \epsilon_{33} \\ \gamma_{23} \\ \gamma_{31} \\ \gamma_{12} \end{Bmatrix} = \begin{bmatrix} \frac{1}{E_{11}} & -\frac{\nu_{12}}{E_{11}} & -\frac{\nu_{13}}{E_{11}} & 0 & 0 & 0 \\ -\frac{\nu_{12}}{E_{11}} & \frac{1}{E_{22}} & -\frac{\nu_{23}}{E_{22}} & 0 & 0 & 0 \\ -\frac{\nu_{13}}{E_{11}} & -\frac{\nu_{23}}{E_{22}} & \frac{1}{E_{33}} & 0 & 0 & 0 \\ 0 & 0 & 0 & \frac{1}{G_{23}} & 0 & 0 \\ 0 & 0 & 0 & 0 & \frac{1}{G_{31}} & 0 \\ 0 & 0 & 0 & 0 & 0 & \frac{1}{G_{12}} \end{bmatrix} \begin{Bmatrix} \sigma_{11} \\ \sigma_{22} \\ \sigma_{33} \\ \tau_{23} \\ \tau_{31} \\ \tau_{12} \end{Bmatrix} \quad (2.1)$$

For a thin lamina under a plane stress state, the elastic constants necessary to define the mechanical behaviour are  $E_{11}$ ,  $E_{22}$ ,  $\nu_{12}$  and  $G_{12}$ . Researchers have developed and proposed various experimental approaches and methodologies for calculating the relevant mechanical parameters of composite materials. Most are grouped in several experimental standards (ASTM, ISO, CEN), including testing conditions in various diverse environments (Ahmed et al., 2021). The Tensile Test (TT) is the most often used approach for composite characterisation since it uses a primary type of sample for testing and allows for the acquisition of all the mechanical characteristics mentioned before. It facilitates the computation of stress-strain behaviour and modulus of materials and a comprehensive mechanical assessment, including ultimate tensile strength, breaking strength, elongation, and additional mechanical properties such as Poisson ratio, yield strength, and stiffness characteristics. The ASTM D3039, 2014 standard is the most widely used in academia and industry for performing the Tensile Test on polymer matrix composite materials reinforced with high/modulus fibres, aiming to measure

the values of strength mentioned before. The test supposes a thin flat strip of material with a constant rectangular cross-section clamped with a set of universal mechanical testing machine grips and uniformly loaded in tension. At the same time, the force and deformation are recorded independently. The highest force sustained before failure may be used to calculate the ultimate strength of the material, and the final stress-strain curve can be derived if the strain is tracked using any technique available. The ultimate tensile strain, the tensile modulus of elasticity, and Poisson's ratio may all be calculated from this final curve.

Various testing options are available in addition to tensile tests for determining the quality of composite materials, specifically in the directions 22 and 12, where non-linear behaviour might be present as matrix-dominated properties. A comprehensive characterisation involves obtaining the entire stress-strain curve until failure. Unfortunately, in many research cases, specific tests may not yield the whole curve, or even worse, the final result may be strongly influenced by the early appearance and interaction of various failure modes (Saba et al., 2019) (e.g. matrix cracking and ply delamination). Regarding these limitations, examining some other convenient, standardised methods for polymer composites, such as flexural, shear, and compression testing, in addition to tensile tests, is feasible.

- Compression Test

Composite compression testing methods involve applying a compression force to thin and flat rectangular test specimens using three ways (Figure 2.3): end loading (ASTM D695, 2015), shear loading (ASTM D3410, 1987), and combination loading (ASTM D6641, 2014). End loading applies the entire load to the flat end of the specimen, whereas shear loading applies the tab faces of the specimen, and combined loading refers to the combination of shear and end loading. The resulting stress-strain diagram of compression testing offers the material's elastic limit, proportional limit, and yield strength, all of which are vital insights into the material's behaviour under a crushing load. Compression testing fixtures use rectangular wedges for varied specimen widths and thicknesses. Upper and lower wedge housing block assemblies hold each set of specimen grips. The wedges are available in various thicknesses, enabling the evaluation of specimens of differing thicknesses. The wedge grips' outer edges are equipped with notches to accommodate end bars allowing shear-loading or end-loading. The test machine's upper wedge housing block assembly is attached to the upper crosshead, while the lower one rests on a lower plate. In addition, the end bars facilitate uniform movement of each wedge of a pair during specimen loading, minimising specimen bending (according to ASTM D3410, 1987). The compression of composite laminates and the investigation of its many failure mechanisms have been extensively studied, as evidenced by several published works (D. Liu et al., 2022; Vogler et al., 2000).

- Flexural Test

While doing a flexural test, the specimen will typically be positioned to lie on a support span. The load will then be given to the centre of the specimen by the loading nose, resulting in three points bending at a predetermined speed (See Figure 2.4). The support span, the speed of the loading, and the maximum deflection are the parameters contemplated during the test, which are commonly determined regarding the thickness

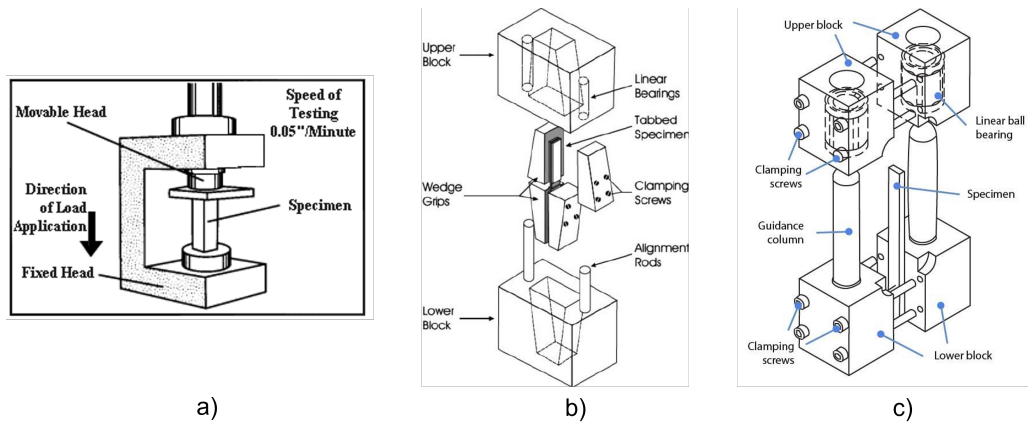


**Figure 2.3:** Schematic representation of the different testing procedures for the compressive test: a) End Loading, b) Shear Loading, c) Combined Loading.

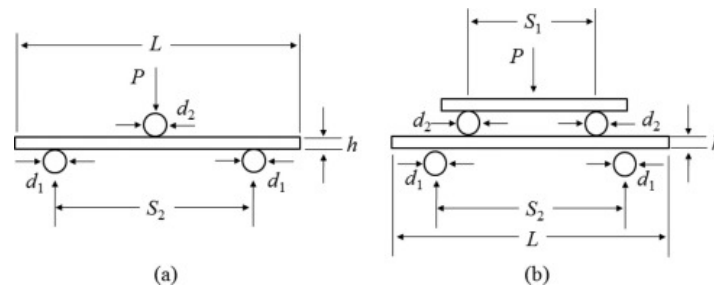


**Figure 2.4:** Most typical types of bending tests in the literature: a) Three-Point Bending Test and b) Four-Point Bending Test. Both correspond to the standard ASTM D7264, 2015.

of the test specimen, and their definition is dependent on the standard that is being taken into account (ASTM D7264, 2015). The results of this test are usually based on the homogeneous isotropic beam equation, which, for laminated composites, it needs to be changed to take into account the stacking sequence of the individual plies. These calculations make it feasible to describe the modulus and strength of laminates manufactured using angle-ply orientations. The literature contains in-depth analyses of the flexural test utilised on FRP materials (Browning and Mair, 1974; Nunes et al., 2002).

- Shear Test

In the quest for more reliable results with processes requiring less time and effort, shear testing may be the most investigated test for laminated composite materials. The number of possible configurations is additionally influenced by the fact that shear operates in a laminate on more than one plane and that the interaction between the laminate's fibres and resin can vary concerning the shear plane. These procedures are divided into in-plane shear testing and interlaminar shear tests. The primary goal of all available procedures is to determine shear modulus and shear strength, providing either qualitative or quantitative data. The optimum quantitative shear test technique should provide a pure, homogenous shear stress zone.

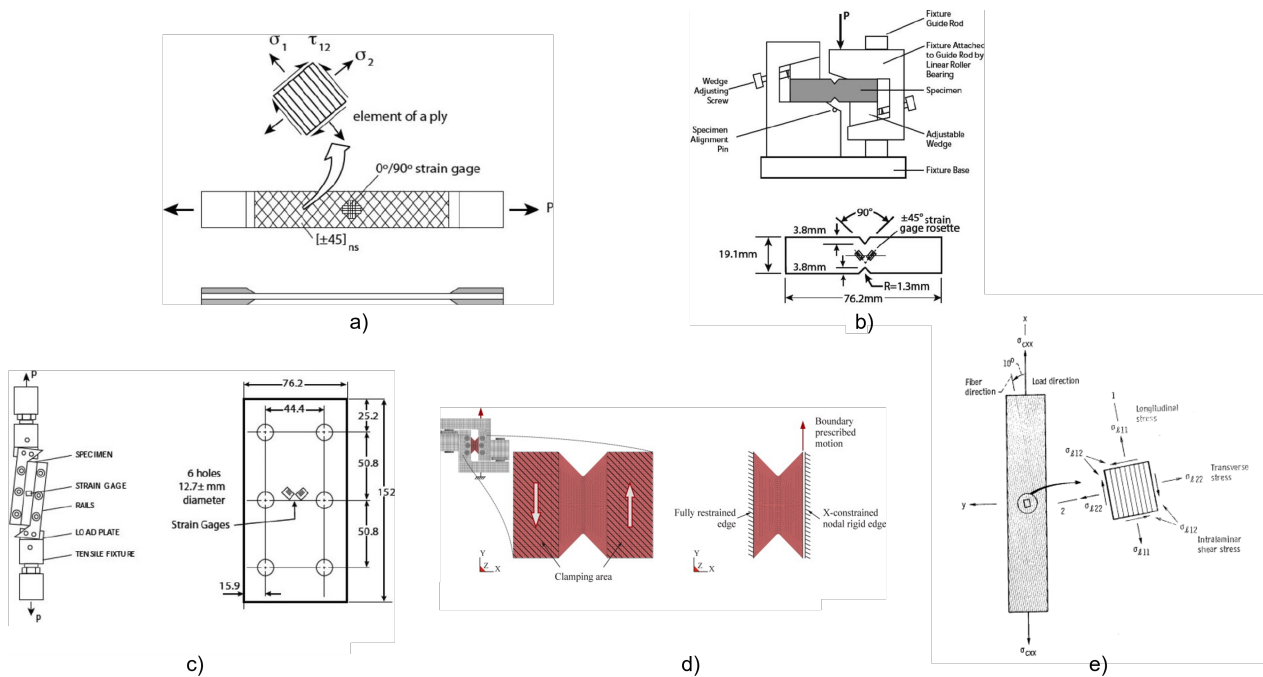


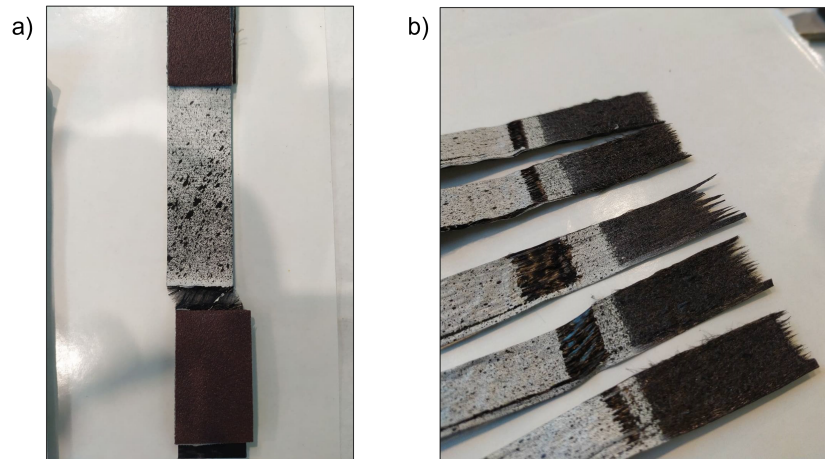
**Figure 2.5:** Different Shear Test methods available in the literature: a)  $\pm 45^\circ$  off-axis Tensile Shear Test, b) V-Notched Test, c) Rail Shear Test, d) The Iosipescu and e)  $10^\circ$  off-axis Tensile Shear Test.

Moreover, the applied load and the shear stress amplitude in the test portion should have a different connection. Also, the test portion should be the most subjected to shear stress compared to all other parts of the specimen for reliable evaluation of the shear stress/strain response. Apart from the  $\pm 45^\circ$  off-axis tensile test (ASTM D3518, 2007), the most frequent shear tests used by researchers include the V-notched test (ASTM D7078) (Adams et al., 2007; D7078, 2005), the rail shear test (Whitney et al., 1971), the Iosipescu (ASTM D5379) (Broughton et al., 1990; D5379, 2012), and the  $10^\circ$  off-axis tensile (Y. Wang, Chea, Belnoue, et al., 2020). There are comparison and review studies on all of these shear test methods accessible in the literature (S. Lee and Munro, 1986).

## 2.3 Mechanical characterisation of uncured prepreg laminates

### 2.3.1 Intraply behaviour of uncured prepreg laminates

Tensile tests were first carried out since they were estimated to be the most accurate and straightforward for mechanical characterisation. In the initial inspection, the transverse tensile test presented a few inconveniences with a non-linear response followed by an early fracture of the sample because, in its uncured state and with this fibre configuration, the resin is not capable of withstanding high levels of loads and the fibres separate very easily as shown in



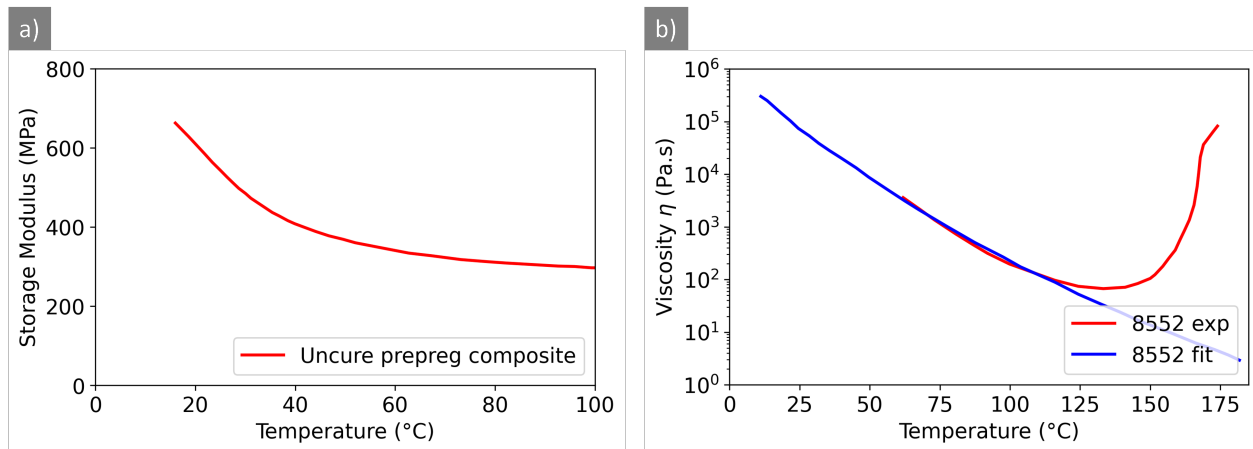
**Figure 2.6:** Typical failures of uncured prepreg coupons: a) Transverse Tensile samples ( $[90^\circ]$ ) fail due to the resin's poor strength resistance, and b) Longitudinal Tensile samples ( $[0^\circ]$ ) consistently fail at the tab zone.

Figure 2.6a. When temperatures of  $40^\circ\text{C}$  and  $60^\circ\text{C}$  were applied, the heating process strongly impacted the coupon behaviour. In this situation, the specimens are tested using a universal testing machine equipped with a thermal chamber. The cartridge heaters will generate heat, which a fan will distribute evenly throughout the chamber. This process typically takes between 10 and 15 minutes to uniformly heat the sample, clamps, and all other components within the chamber. Most of the specimens demonstrated significant deformation due to the heating process, as the reduction in the resin's viscosity caused the samples to deform under their weight. This phenomenon was mitigated immediately by including a pre-loading phase during the experimentation. However, some of the specimens exhibited premature failure, thereby obstructing the reproducibility of the test.

On the other hand, the tensile test results in fibre directions (Normal Tensile Test) showed a linear response, just as was anticipated. However, there was a recurrent tab failure as presented in Figure 2.6b. This phenomenon happens because the uncured resin can not be compressed; therefore, when the testing machine clamps are closed, a strong grip is never achieved since the material stretches and squeeze within the grip. In conjunction with the significant amounts of load that the fibres can support, this behaviour results in the tabs detaching from the grips, thereby interrupting the test.

The shear tensile tests appeared to have a usual outcome, characterised by a non-linear response and a viscoelastic effect. Further investigation revealed inconsistencies in the interaction and bonding between the plies. This fact led to an improper distribution of the stress within the sample rendering the invalid test results. These abnormalities in all the tensile tests triggered the hunt for an explanation of this inaccuracy and its potential link with the state of the resin, preceded by the quest for a solution.

The potential solutions must account for the operating temperatures in our case study. Since this investigation is motivated by the thermoforming manufacturing process, the environmental conditions involve temperatures of  $20^\circ\text{C}$  (henceforth referred to as "RT" or



**Figure 2.7:** a) Dynamic Mechanical Analysis of a prepreg sample subjected to periodic cantilever beam deflection and b) Temperature dependence of the 8552 epoxy viscosity.

"Room Temperature"), 40°C, and 60°C. To acquire a preliminary understanding of the material's response to this temperature change, a Dynamic Mechanical Analysis (DMA) was first performed. Figure 2.7a shows a DMA test of one AS4/8552 prepreg, demonstrating that the storage modulus of the material drops by up to 80% between ambient temperature (20°C) and 100°C.

This severe behaviour change is attributed to the uncured state of the composite material's resin. Due to the fluid-like nature of the uncured resin, its viscosity will be significantly affected by temperature. The manufacturer provided a viscosity versus time chart that considered temperatures between 60°C and 180°C. This data was then fitted and modified with a mathematical function to produce viscosity values for the temperature range considered in our case study. The viscosity of the 8552 epoxy resin was determined and is shown in Figure 2.7b, along with the numerical approximation. An Arrhenius law was employed (Equation 2.2), where the coefficients of the fitting are  $B = 2.06 \times 10^{-10}$  Pa · s and  $C = 7.94 \times 10^4$  J/mol.

$$\eta(T) = B \exp\left(\frac{-C}{RT}\right) \quad (2.2)$$

This preliminary study outlines the starting conditions of a material with significant temperature sensitivity, poor linking between plies, and semi-solid behaviour that leans more towards fluid than solid, allowing for a high percentage of compaction. In order to prevent the tab from compressing and detaching from the grip in the case of the normal tensile test, it was decided to cut down on the total amount of prepreg plies included inside the laminate. It was found that the number of plies was also altering the stress response of the sample (see Figure 2.8). However, it was instantly attributed to the tab zone's poor grip rather than any other effect that depended on the laminate structure. Eventually, a reliable result was produced by considering both one and two prepreg layers. This result was the same for both samples and of the same magnitude as the values reported in the datasheet provided by the manufacturer.

Because of the experimental difficulties to fully characterise uncured prepreps by standard

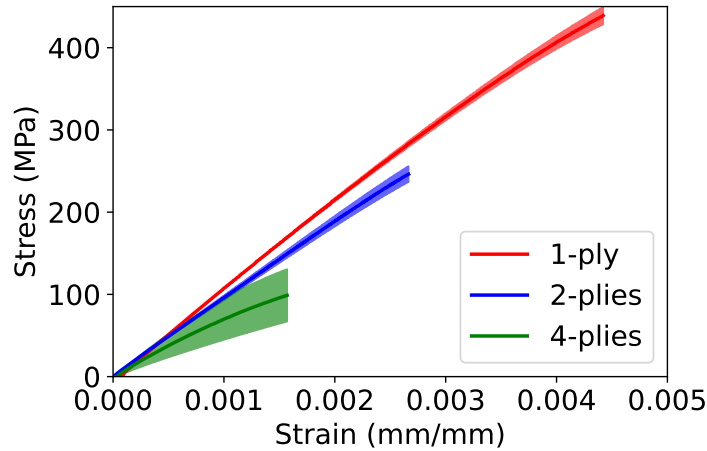


**Figure 2.8:** Stress-strain response of Normal Tensile test while modifying the thickness of the laminate by using 1, 2, and 4 plies.

methods, it was decided to look into alternative types of experimental shear tests because decreasing the number of plies for the  $\pm 45^\circ$  tensile test samples is not an option owing to the requirement for symmetry in the sample, which must be achieved by using at least four plies and results in the same issue as before with a poor grip on the tab.

The first shear test attempted was an adaption of the Double Notch Shear Test since the configuration requires a universal testing machine and does not require an additional fixture, as with other types of shear tests. The adaptation comes from the fact that this test is originally performed in compression; however, it cannot be carried out in this manner for our case study because soft uncured prepreg laminates do not support compressive loading and will buckle than suffer an in-plane shear fracture. The sample used has the same dimensions as the one for the tensile test. The test configuration includes two notches opposite located along the thickness with the same length that, during the tensile loading, would cause shear stress in the plane 1-3 (regarding the same coordinate system mentioned in section 2.2) of the sample. Since the initial instance of loading, a significant amount of fibre bridging within the open fracture was observed (Figure 2.9a), which is known to affect the measured strength significantly (Russo et al., 2019). Raising the temperature and eliminating the influence of the resin on the stress response only complicated the problem since the response produced was entirely influenced by the evolution of the fibre-bridging effect during testing. The variable amount of fibre-bridging made it challenging to produce repeatability, invalidating the test for the case of uncured prepreg composites.

The  $10^\circ$  off-axis test (Y. Wang, Chea, Belnoue, et al., 2020) was also considered while searching for a reliable experimental test to assess the in-plane shear behaviour of uncured UD thermoset prepreg composites. This test employs tensile samples with fibres at  $10^\circ$  relative to the loading axis to generate a shear band area as shown in Figure 2.10 a). Some of the fibres are not fully clamped at both ends of the sample, and applying tensile stress will form a heavily sheared zone in the centre. Calculating the associated shear stress involves converting the applied stress state in the global coordinate system to a local coordinate system represented by the

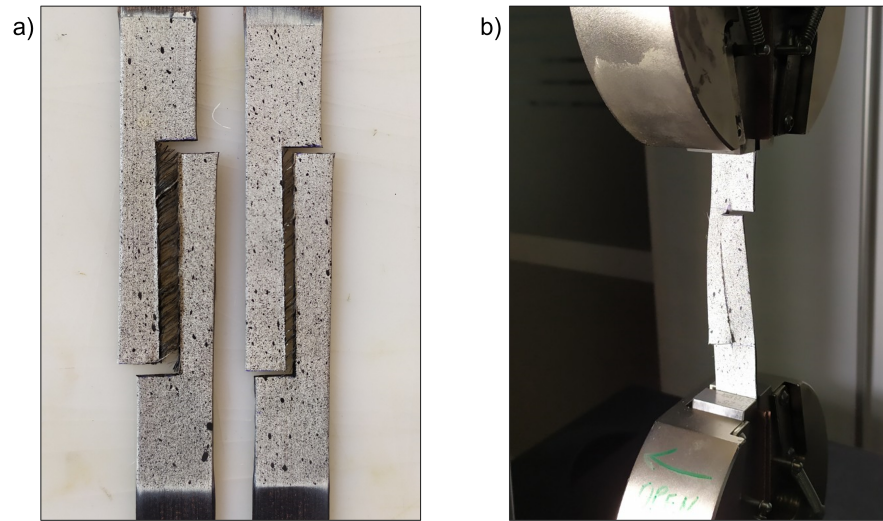


**Figure 2.9:** Double Notched Test modification for uncured prepreg composite samples: a) The presence of fibre bridgings in the samples, and b) The torsion effect caused by the fibre bridging.

local axis 1, indicating the orientation of the fibres. Although the test setup is uncomplicated, there were discovered to be certain restrictions placed on the equipment configurations that may be utilised at our facilities. The dimensions of the sample may need to be excessively large to satisfy the requirement of a non-clamped fibre zone with  $10^\circ$  of inclination in the middle of the sample. This may present a problem for specific testing configurations, as a large sample may not be accommodated within the testing machine. The shorter example given by Wang Y. Wang, Chea, Belnoue, et al., 2020 has dimensions of  $260 \times 40 \text{ mm}^2$  and a thickness of 6 mm, excluding tabs. Under the scenario for room temperature, there does not impede to carrying out the test; however, the challenge arises when the thermal test chamber is mounted with the universal testing machine because there is a constrained distance between the clamps, as shown in Figure 2.10b. With a width of this magnitude, the required clamps have a considerable dimension, further constricting the available span. When the test setup was completed, the largest span accessible between the clamps was between 150 and 200 mm. This distance is insufficient for conducting the test with a maximum displacement of 15 mm for the sample that was specified in the publication. One potential solution was to narrow the sample, which would, as a side effect, also shorten its length. The disadvantage of this solution is that it would result in a lower load being supported, which, in the previous scenario, was already very close to the limit of the minimum amount that could be accurately measured by the load cell.

Despite the inconveniences found, the experiment was conducted using a sample of dimensions  $180 \times 17.5 \times 0.4 \text{ mm}^3$ , following necessary adjustments to the equipment and sample. The experiment outcomes are displayed in Figure 2.10 c). The minimum capacity load cell available at our facilities was 500 N and has been designed to accommodate small clamps with a tabbed zone measuring  $20 \times 20 \text{ mm}$ . Certain sections of the sheared zone were observed clamped when the sample was reduced to its minimal dimension. The present action can result in an elevation of the load under measurement, as certain fibres may experience normal stress

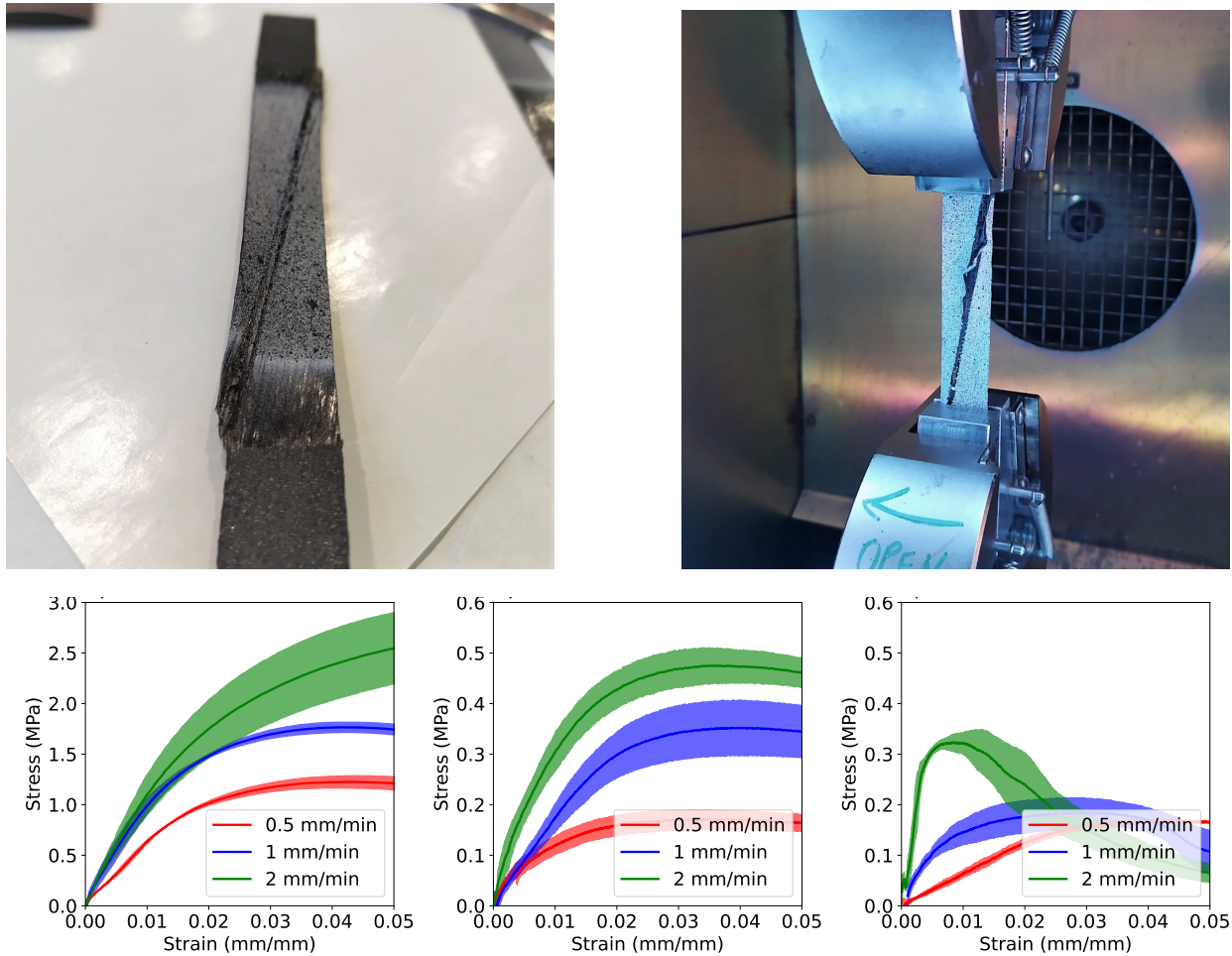


**Figure 2.10:** 10° off-axis Tensile Shear Test of uncured prepreg composite laminates. a) Test sample displaying the 10° inclination of the sheared zone after testing. c) Test results at three temperatures (RT, 40°C, and 60°C) and three displacement rates (0.5, 1, and 2 mm/min).

instead of shear stress. The samples exhibited a significant presence of fibre bridging while also demonstrating compliance with the expected viscoelastic behaviour of the material.

At the same time, as different methods for in-plane shear measurement were offered, interest in exploring the physics of the interaction between plies inside the sample grew. In addition to the fact that the failure of the tab is related to the large amount of force resisted by the sample and the compacting of the material, the uniform distribution of the load inside the sample was also in question. The  $\pm 45^\circ$  tensile test was analysed similarly to the normal tensile test, with the suspicion that slippage was occurring between the plies. The stacking sequence  $[\pm 45]_{ns}$  was applied to samples with  $n$  values of 2, 4, and 8. Non-homogeneous load distribution was demonstrated because altering the sample's thickness affected the stress response. A subsequent DIC examination indicated that the sample did not have a zone with a concentration of strain and stress, as is often the case with tensile testing. Instead, the

sample had several different zones where the strain and stress were concentrated, and these zones varied. These discrepancies may result from numerous plies slipping into the sample, resulting in varying concentrations during the test. Now, efforts were focused on preventing these slipperinesses and creating a uniform load distribution inside the sample.

### 2.3.2 Partial curing device

Exploring the more used standard methods and observing the material's behaviour when subjected to different loading conditions and configurations helped to identify specific aspects of uncured prepreg composite materials. The primary challenge to be addressed in order to perform mechanical characterisation using conventional methods is the poor inter-ply adhesion that these laminates exhibit. The present section describes a novel sample preparation method, including partial curing of the specimen edges compatible with the standard tensile tests used for the mechanical characterisation of prepreg laminated composites.

The fact that the averaged stress carried by a tensile uncured laminated sample was strongly dependent on the number of plies of the laminate is a consequence of the easy slippage between the plies during the deformation. For a tensile coupon, the load is transferred from the testing frame to the specimen by shear until uniform stress conditions are attained. For cured laminates, the transfer length is usually small, of the order of the width of the laminate; however, for uncured prepreg, ply-ply sliding and intraply shear behaviour dominates the stress transfer making it difficult to assume uniform stresses in the gauge length of the coupon.

The challenge was to constrain the plies to experience the same displacement together. This would prevent a non-homogeneous distribution of the load. Since the characterisation of uncured prepreg composites does not have precedence, it was not feasible to rely on existing approaches that would be accessible in the literature and lead to several potential solutions. Improving the stress transfer by through-the-thickness screw connections or stitching will result in stress concentrations and failure. While using some adhesive between each ply makes sense, producing many samples will be time-consuming and laborious. As the prepreg composite already contains a component that will fuse the plies, it will be opportune to take advantage of this material's characteristics; all that needs to be done is to activate this resin in the region that is of interest.

The task requires the resin to be cured only in the tab sections while maintaining a portion of the sample with uncured material, the gauge length. This methodology will be called in the thesis partial curing approach. This premise is the motivating concept behind designing a novel production mechanism that allows for mechanical characterisation without the previously mentioned disadvantages. This will enable the sample to be securely clamped to the testing equipment without compressing the plies, ensuring that each ply undergoes the same displacement because the shear stress is securely transferred from the grips to the coupon. The stress and strain will be centred on an area of the sample containing uncured material, enabling the calculation of the desired mechanical parameters.

Figure 2.11 provides a general sketch of the novel system designed to create the specimens. A square aluminium plate is used as a compaction tool. Six parallel cylindrical conducts for heat and cold sources are drilled through the plate. Four cartridge heaters with a length of

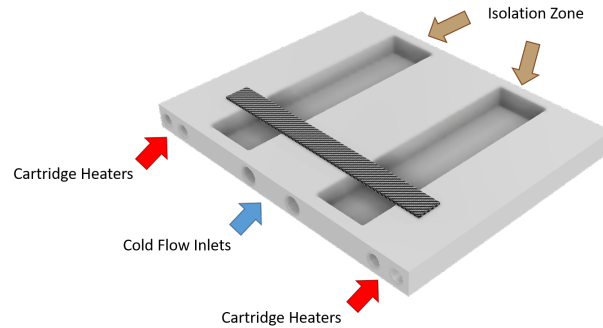


**Figure 2.11:** Partial curing device to produce multiaxial tensile coupons for mechanical characterisation.

150 mm, a diameter of 10 mm, and a power of 650 W each were placed on the two edges of the plate. An FP50 Julabo refrigerated/heating circulator with a heat capacity of 2 kW and a flow rate of 25 l/min circulates a cooling liquid through the two conducts in the centre portion of the plate. In this manner, the centre part of the specimens is kept at a temperature of  $\approx 18\text{ }^{\circ}\text{C}$  while the specimens attain a temperature of  $\approx 100\text{ }^{\circ}\text{C}$ . Two sockets were machined between the curing and cold zones, replacing the aluminium with Celotex prisms functioning as heat insulators.

With a starting fluid temperature of  $-20\text{ }^{\circ}\text{C}$ , the operation begins by cooling the plate's central region, eventually achieving a surface temperature of  $-8\text{ }^{\circ}\text{C}$ . After that, the heat is applied with a preset temperature of  $180\text{ }^{\circ}\text{C}$  so that the ultimate temperature distribution would be  $\approx 100\text{ }^{\circ}\text{C}$  on the edges to be cured and  $\approx 18\text{ }^{\circ}\text{C}$  in the coupon centre. The temperature of the specimens was controlled at a stable level by employing thermocouples attached to the external surface. The method of calibrating the temperature on the plate was optimised, resulting in cooling and heating, achieving the best efficiency. When the heating region is first activated, the stabilisation time is about two to three times longer than what was attained in the previous case. When the plate has been heated and cooled, the surface of the plate has to be dried because, during the cooling process, water droplets condense on the surface.

The portions of the specimen that were cured at the conclusion of the procedure matched the intended tab dimension, which in our case was  $20 \times 20\text{ mm}^2$ . A Teflon film was placed between the plate and the samples for easy release. Hand layup is used to create the composite plates with varied stacking sequences, and the samples are then cut with dimensions of  $200 \times 20 \times 1.65\text{ mm}^3$  corresponding to length, width, and thickness, respectively. Since cutting the samples while the prepreg is uncured is more straightforward, they must be cut before being cured. After this step, the specimens were positioned on the aluminium stage and sealed inside a vacuum bag system for about six to eight hours while the vacuum pump operated. Following this period, the specimens could be removed without much effort, although careful management was required to minimise any bending or twisting effects. The experimental setup detailed in this research allows for producing five specimens throughout each manufacturing process cycle. This innovative approach produced suitable specimens for

the mechanical characterisation of prepreg composite in an uncured state, and the method has the potential to be applied to other types of characterisations or qualitative analyses, as well as to the development of new standards for testing uncured composite materials.

At first, the identical  $\pm 45^\circ$  tensile test evaluation described in the last portion of section 2.3 was used to verify the process and show a proper stress response of the sample regardless of the number of plies considered. Samples with a stacking sequence of  $[\pm 45^\circ]_{sn}$  were created with  $n$  values ranging from 2,4 to 8, undergoing the previously indicated partial curing method. Figure 2.12 a) and b) compares the strain-stress response for uncured and cured tab samples, demonstrating that the issue of incorrect displacement application to all samples was rectified. The images in Figure 2.12 c) and d) correspond to the strain calculated through the digital image correlation analysis, where it is possible to appreciate the different strain distributions with uncured and cured tabs. Different stress concentration zones are formed during the test in the first, while a unique zone corresponding to the zone of maximum stress and strain concentration can be observed in the second.

The samples and the corresponding stacking sequences for the tensile tests Normal (L), Transverse (T), and In-plane Shear (IPS) ( $\pm 45^\circ$  off-axis shear) are represented as  $[0^\circ]_8$ ,  $[90^\circ]_8$ , and  $[\pm 45^\circ]_{2s}$ , respectively (see Figure 2.13). The L, T, and IPS specimens were tested using an Instron 3384 universal testing machine with a thermal chamber coupled at three temperatures (RT,  $40^\circ\text{C}$ , and  $60^\circ\text{C}$ ), taking into consideration the guidelines established in the ASTM standard methods D3039, 2008 for the normal and transverse tensile tests, and D3518, 2007 for shear, tensile tests. Five samples per condition were employed to address the averaged value and dispersion of mechanical behaviour. To record the load, a load cell of 10 kN for L tensile and 500 N for T and IPS tensile was used. Controlling the machine stroke allowed each test to be carried out at a constant strain rate. The used samples have a final thickness of 1.65 mm after being compacted from 8 plies, which is thicker than the required thickness of 1.5 mm per the standard D3039, 2008. The Normal Tensile test (L) was conducted at a unique displacement rate of 1 mm/min because, in the direction of the fibres, the material does not exhibit a viscoelastic effect; however, the temperature does reduce the material's strength.

The evaluation of stress and strain in the loading direction ( $x$  is the specimen long direction and  $y$  is the in-plane perpendicular) allows the determination of the longitudinal L ( $\sigma_x = \sigma_{11}$  and  $\epsilon_x = \epsilon_{11}$ ) and transverse T behaviours ( $\sigma_x = \sigma_{22}$  and  $\epsilon_x = \epsilon_{22}$ ), with respect to the used specimen during the test. The stress in the loading direction is calculated as follows:

$$\sigma_x = \frac{F}{A} \quad (2.3)$$

The equation 2.3 represents the relation between the stress ( $\sigma_x$ ), the load ( $F$ ), and the cross-sectional area ( $A$ ). The DIC method was utilised for measuring strain  $\epsilon_x$ , as further described below. In the context of shearing forces, stress and strain are referred to as in-plane shear stress ( $\tau_{12}$ ) and ply shear strain ( $\gamma_{12}$ ), respectively. The determination of these shearing properties was adapted to the IPS test by Rosen Rosen, 1972. Based on an equilibrium argument, the author demonstrated that, given the existence of a state of constant stress, the average in-plane shear stress can be expressed as:

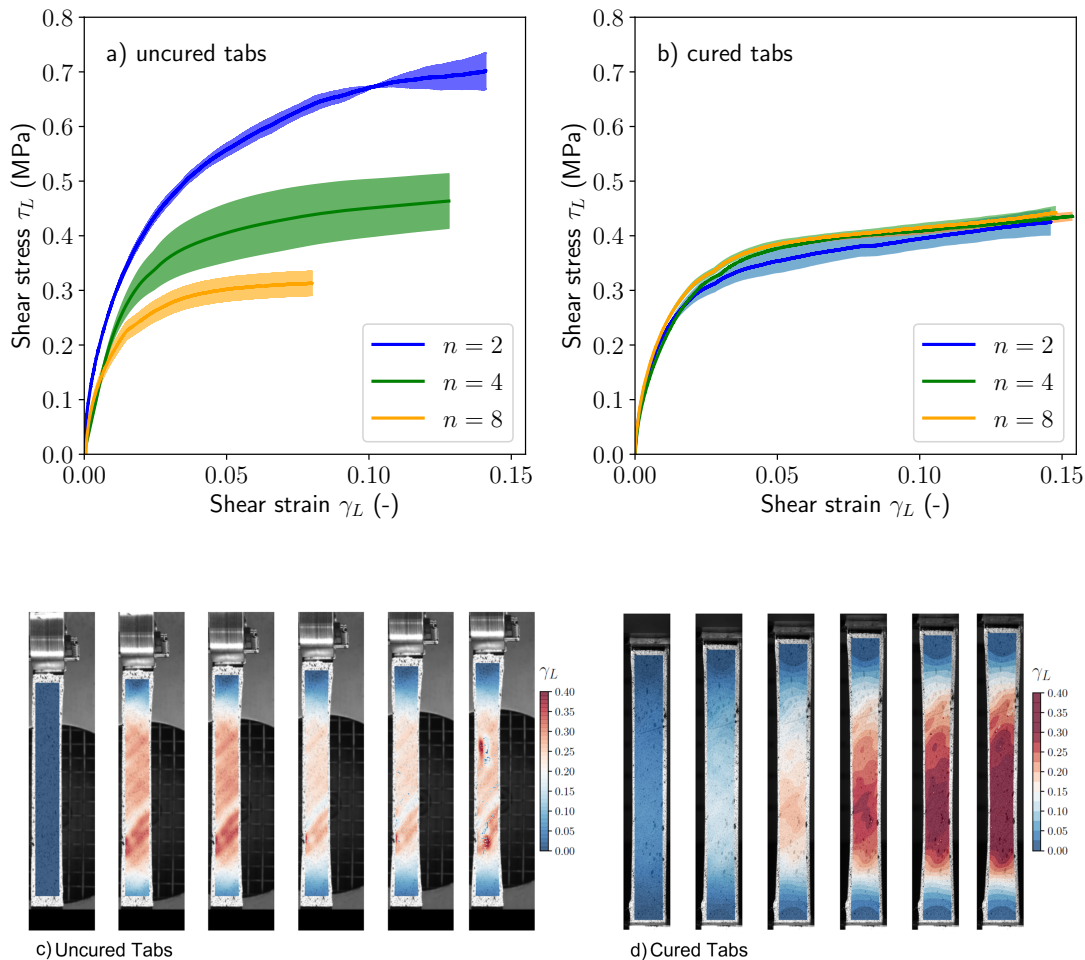


**Figure 2.12:**  $[\pm 45^\circ]_{ns}$  tensile tests ( $n = 2, 4, 8$ ): a) specimens with the uncured gripping area, b) specimens with the cured gripping area, c) DIC analysis of samples 16 plies and uncured tabs and, d) DIC analysis of samples 16 plies and cured tabs.

$$\tau_{12} = \frac{F}{2A} = \frac{\sigma_x}{2} \quad (2.4)$$

Rosen formulated the ply shear strain concerning the axial strain ( $\epsilon_x$ ) and transverse strain ( $\epsilon_y$ ) by axis rotation following the Mohr's circle as:

$$\gamma_{12} = (\epsilon_x - \epsilon_y) \quad (2.5)$$

The strain measurement was carried out with DIC digital image correlation (Vic2D by Correlated Solutions). To this end, the specimen surfaces were painted white and then sprayed with black dots to produce the speckle pattern necessary for image correlation. A 2 MP camera was used to acquire images of the deformed specimens at two images per second, one image per second, and one image every two seconds, according to the considered displacement

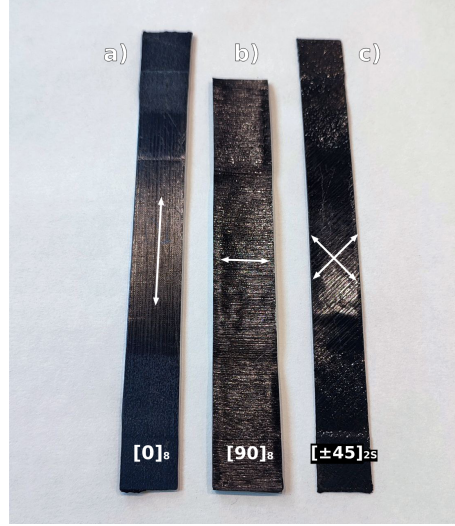


**Figure 2.13:** Tensile test samples after curing the tabs: a) Normal tensile test with stacking sequence of  $[0^{\circ}]_8$ , b) Transverse tensile test with stacking sequence of  $[90^{\circ}]_8$ , and c)  $\pm 45$  stacking - curing shear tensile test with stacking sequence of  $[\pm 45^{\circ}]_{2s}$ .

rate. The region of interest (ROI) for the strain measurements was rectangular of  $60 \times 20 \text{ mm}^2$  centred in the middle of the specimen. After finishing the tests, digital image correlation is carried out, and the averaged values of the Logarithmic Euler-Almansi surface strain tensor  $\mathbf{e}_l = \frac{1}{2} \log(\mathbf{F} \cdot \mathbf{F}^T)$  obtained within the ROI. The engineering components  $\bar{\epsilon}_x$ ,  $\bar{\epsilon}_y$  and  $\bar{\epsilon}_{xy}$  were also determined from the  $\mathbf{E}$  tensor components as:

$$\bar{\epsilon}_x = \sqrt{1 + 2E_x} - 1, \quad \bar{\epsilon}_y = \sqrt{1 + 2E_y} - 1 \quad \text{and} \quad \bar{\epsilon}_{xy} = \sin^{-1} \frac{2E_{xy}}{\sqrt{(1 + 2E_x)(1 + 2E_y)}} \quad (2.6)$$

### 2.3.3 A rheometer-based tensile test

Despite successfully resolving the issue of interply slippage, the transverse specimens continued to experience significant deformation when subjected to testing conditions of  $40^{\circ}\text{C}$  and  $60^{\circ}\text{C}$  during the heating process. The presence of cured tabs on both sides of the sample did not prevent the occurrence of this defect, as the sample continued to experience deformation due to its weight in the uncured areas. The issue was found to be closely linked to both the vertical positioning of the specimen during the heating procedure and its overall weight. Therefore, any potential solution must rectify one of these aspects. Modifying the sample's dimensions was a more feasible solution, as altering the positioning of the sample during testing required the modification of multiple fixture setups, resulting in a more challenging task. Consequently, the decision was made to conduct the test on a reduced scale. Various studies in the scientific literature utilise rheology as a means of estimating the mechanical properties of diverse materials (Hsissou et al., 2020; Yokohara et al., 2011). In our case, the used rheometer allowed us to perform tensile tests for small loads.

Rheometry is an essential tool in material characterisation, including various experimental approaches aimed at measuring the rheological characteristics of materials. These features clarify

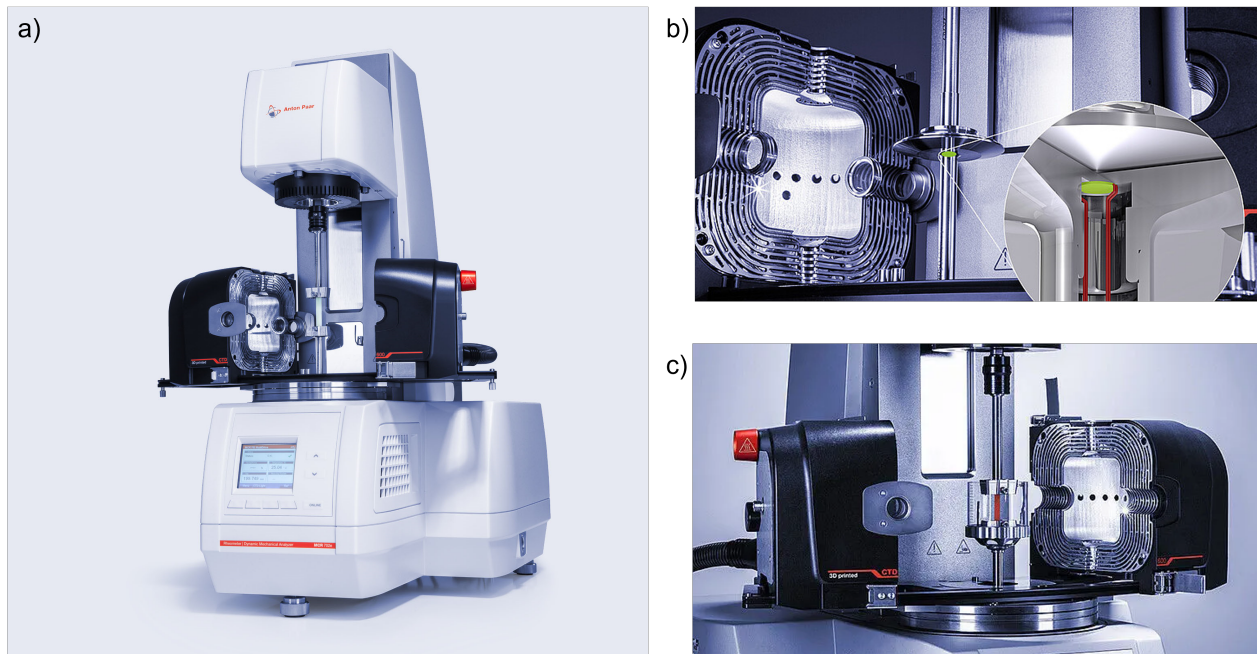


**Figure 2.14:** Rheometer apparatus for tensile tests: a) Modular Compact Rheometer MCR 702e, b) Temperature sensor positioned directly within the measurement system, and c) High-precision temperature control device with optoelectronic technology.

the qualitative and quantitative connections among stresses, strains, and their derivatives, thereby providing significant conclusions about the material's flow behaviour.

The Modular Compact Rheometer MCR 702e (Anton Paar) was selected since it is a sophisticated facility that provides precise manipulation and precise measurements in the field of rheological analysis (see Figure 2.14). The product is furnished with state-of-the-art technology and a modular structure, which provides adaptability in selecting and integrating various accessories and measuring systems. The capacity for adaptability allows for the characterisation of a broad spectrum of materials and the implementation of various rheological evaluations. The rheometer offers researchers a wide range of measurement modes, including steady shear flow, small-amplitude oscillatory shear, and extensional flow, which enables the execution of a tensile test.

Tensile testing with the MCR 702e Rheometer requires multiple successive phases. To begin, a representative sample is carefully created, in the shape of a rectangular strip with dimensions adapted for testing. A sample size of  $20 \times 5 \times 0.75 \text{ mm}^3$  (length, width, and thickness, respectively) was used for this experiment, the samples are depicted in Figure 2.15. During the sample preparation procedure, great care is taken to guarantee consistency and repeatability. Once the sample has been prepared, it is securely put on the MCR 702e Rheometer's specialised clamping mechanism. This clamping device is intended to offer precise sample alignment and fixation during the tensile test. The MCR 702e Rheometer enables the initial specification of the displacement rate, allowing for exact control of the deformation process. The test is conducted until a strain value greater than 0.15 is obtained. This ensures the sample is deformed enough to assess its mechanical characteristics reasonably. Each test

is performed for three samples in order to prove the repeatability of the results. The MCR 702e Rheometer continually captures real-time data on different parameters throughout the tensile test, including applied force, strain, and other pertinent measures.

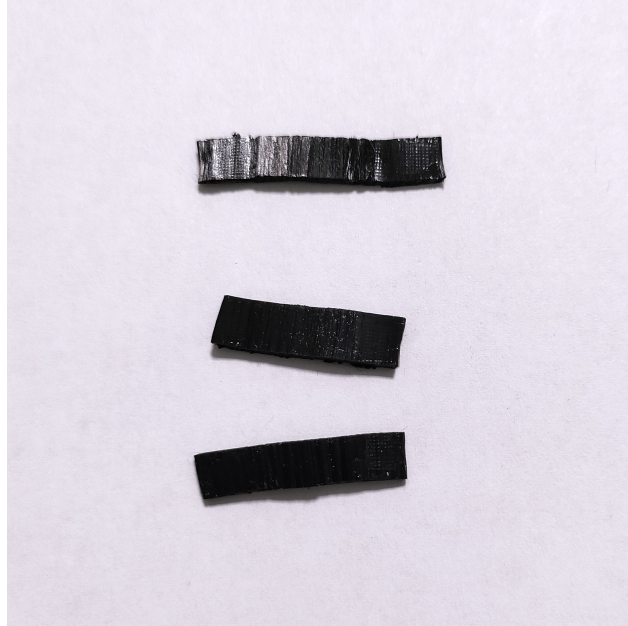


**Figure 2.15:** Samples used in the rheometer-based tensile test. A sample after testing is shown on top, while two untested samples are seen at the bottom.

Given that this method was chosen to conduct tensile tests between 40°C and 60°C, a high-precision temperature control device is employed in conjunction with the rheometer. This gadget employs optoelectronic technology, allowing contactless data transfer through light emission and the photovoltaic effect. Temperature can be monitored without altering torque sensitivity in Separate Motor Transducer (SMT) or counter-movement modes. The sensor is placed directly in the measurement system, near the sample (just one mm far from the specimen), reducing any offsets between the sample temperature and the temperature recorded at the sensor. This allows for precise temperature measurement even during step-like or ramp-like temperature increases. Furthermore, room temperature experiments were conducted using the rheometer to verify the findings obtained at the macroscale level and to ensure that the test results are not affected by any size-related factors that may impact the final curve values.

## 2.4 Mechanical characterisation of interply behaviour of uncured prepreg composites

### 2.4.1 Pull-out test and friction measurements

The simultaneous application of the temperature and the external pressure during the thermoforming of uncured prepreg laminates allows relative sliding between the plies enabling

an easy adaptation of the laminate to the geometry configuration imposed by the tool. This relative sliding between the laminate plies is called friction and represents the force that resists the relative motion between the plies. In the fibre direction, prepreg sheets cannot be stretched, resulting in manufacturing defects during its adaptation to complex geometries, typically wrinkles (Boisse et al., 2018; Guzman-Maldonado et al., 2019). The presence of wrinkle defects in laminated components will reduce their mechanical strength and durability to  $\approx 40\%$  (Bloom et al., 2013; Karami and Garnich, 2005). It has been proved that friction resistance plays a critical role in the formation of wrinkles defects in all the possible mechanisms considered in the literature: inter-ply shear (slippage), ply-tool interaction, and ply-ply slipping (J. P. Belnoue et al., 2018a).

Scientific literature offers several works regarding friction influence on the defect generation during thermoforming of thermoset unidirectional (UD) (Ersoy et al., 2005; Larberg and Åkermo, 2011; Liang et al., 2014; Pasco et al., 2019; Sun et al., 2014; L. Wang et al., 2019), thermoplastic UD plies (J. M. Lee et al., 2017; Murtagh et al., 1995; Sachs, 2014; Ten Thije et al., 2011), impregnated woven (Alshahrani and Hojjati, 2017; Fetfatsidis et al., 2013; Rashidi et al., 2019; Sachs et al., 2014) and dry fibres (Cornelissen et al., 2014). Despite the sort of FRC, the study of friction is generally focused on two types of contact: the ply-ply and the ply-tool contacts. Ply-ply contact is usually regarded as the dependence of the shear response on the process conditions (i.e. temperature, pressure, displacement rate) (Rashidi et al., 2020), including the influence of the resin layers on the lubrication regime (Pasco et al., 2019). The ply-tool contact can be treated as a contact event or consolidation case.

Focusing on wet fibre composites, a short review can highlight the principal devices employed for friction measurements. Groves, 1989 studied friction in a thermoplastic structural composite as shear flow. A rheometer dynamic spectrometer consists of two parallel discs where the prepreg plies are disposed of and sheared in the lamination plane by an oscillatory torsion. The dynamic viscosity is related to the steady shear viscosity by applying a Maxwell model to represent the fluid response, and the resistance against shear can be calculated in terms of dynamic viscosity. This case study did not consider the influence of temperature and normal pressure. Ply-pull-out experiment appears in the work of Scherer and Friedrich, 1991 for thermoplastic composites employing an isothermal condition of  $180^{\circ}\text{C}$  and varying slip velocity and lay-up configuration. A single layer was extracted from a pressured stack using a Universal Testing machine with a controlled displacement rate. An influence of the slip velocity and the stacking configuration on friction was reported. This experiment also pointed out the transition from steady to dynamic friction. A similar work was presented by Murtagh et al., 1995, presenting an alternative test whose primary distinction is the employment of a 'friction sledge'. With this fixture, the sample remains fixed while two outer plates or sledges slide parallel to the sample. Although this study aims at the friction response of moulding materials, it shows an alternative method for prepreg composite in further works (Ersoy et al., 2005; Kaushik and Raghavan, 2010; C. J. Martin et al., 1996). All these authors observed an initial coefficient of friction (CoF) peak, assuming a simple Amontond-Coulomb friction behaviour followed by a stable dynamic response. An important aspect to point out is that in some of these cases, the contact area does not remain constant during the test affecting the applied pressure distribution. Gorczyca-Cole et al., 2007 designed a friction test apparatus and test procedure using the ASTM Standard D 1894 as a guide and previous references. The

device is more straightforward than others, and the sample sticks out at both ends of the test area, allowing the sheared area to remain constant and a homogeneous pressure. This last method was preferred by further authors and applied to different types of FRC as woven reinforced thermoplastics (Fetfatsidis et al., 2013; Lebrun et al., 2004; ten Thije et al., 2008), carbon fibre/epoxy UD prepregs (Joven et al., 2013; Larberg and Åkermo, 2011; Sun et al., 2014).

The number of test methods and friction apparatus, combined with a lack of standardised procedures, make it difficult to compare all the available results and reach a concrete interpretation. Nevertheless, most test rigs designed for friction tests consist of metallic plates with attached material, allowing a motion between them with controlled velocity, temperature and normal pressure. Some specific design characteristics must be considered to improve measurements, such as significant and constant surface contact, rigid fixation of the samples to the rig and reasonable control of the pressure and temperature distribution (Sachs et al., 2014). The two methods that can fulfil these characteristics are the Pull-Through and Pull-Out tests, and they have more presence in recent publications (Aveiga et al., 2023; Dutta et al., 2023; Kim et al., 2021; Rashidi et al., 2020).

The pull-out test is used in this study to experimentally analyse and evaluate the friction resistance between ply-ply and ply-tool in different temperature, velocity, and pressure conditions, which represent the conditions during the manufacturing process of thermoset prepregs (Ersoy et al., 2005; Rashidi et al., 2019; L. Wang et al., 2019). It involves applying a tensile force to extract a prepreg sheet between two stationary, rigid plates, which allows for the simultaneous application of pressure and temperature. The pulling sheet can be clamped between the metal prepreg-tool or the prepreg-prepreg contact surfaces. This method is versatile and easily adapted to various material configurations and temperatures (Gorczyca-Cole et al., 2007; Groves, 1989; Morris and Sun, 1994; Scherer and Friedrich, 1991). However, there are various approaches in the literature for introducing clamping pressure and ensuring a uniform action.

The testing apparatus developed in our department is shown in Figure 2.16a. It consists of two simultaneous actuators that regulate the vertical pulling force ( $F$ ) and the horizontal clamping force ( $N$ ). This apparatus is based on fixtures for similar tests as in Kim et al., 2021; Pasco et al., 2019; Sun et al., 2014; L. Wang et al., 2019. The system is mounted on a universal testing frame for pulling the prepreg sheets. At the same time, the clamping force is introduced by a mechanical fixture driven by a compressed air cylinder (Compact Bore 100, Stroke 0100 by Metal Work Iberica S.A.<sup>®</sup>). Four stainless steel guide bars were used to maintain clamping plates parallel during the load application. The clamping plates were machined on 6082 aluminium, where four cartridge heaters were inserted. Each cartridge heater contained a thermocouple in the middle position used to control the temperature of the test with a Eurotherm EFit SCR Power System. An additional thermocouple was placed on each clamping plate's surface to check the tests' effective temperature. An ulterior time of 30 min has waited to stabilise the temperature of the aluminium plate. The pneumatic cylinder was controlled with a PID-controlled servo-valve connected to the air-compressed line. The loads  $F$  and  $N$  were measured using two Instron 100 and 10 kN load cells, respectively.

Figures 2.16b and 2.16c show the two set-up configurations to perform prepreg-tool or prepreg-